Studies on Selective Degradation of Splicing Factor CAPERα by Anticancer Sulfonamides

Studies on Selective Degradation of Splicing Factor CAPERα by Anticancer Sulfonamides

January 2018

Taisuke UEHARA

Studies on Selective Degradation of Splicing Factor CAPERα by Anticancer Sulfonamides

A Dissertation Submitted to

the Graduate School of Life and Environmental Sciences,

the University of Tsukuba

in Partial Fulfillment of the Requirements

for the Degree of Doctor of Philosophy in Biotechnology

(Doctoral Program in Life Sciences and Bioengineering)

Taisuke UEHARA

Contents

Chapter I

Preface

Control over a protein function by small-molecule as a therapeutic approach generally targets a binding site of an endogenous metabolite or a small ligand in an enzyme or receptor protein, respectively. On the other hand, proteins which consist of large protein–protein interaction interfaces and lack a deep pockets, many of transcription factors and splicing factors, are often deemed as an undruggable target in medicinal chemistry[1]. Therefore, targeting protein metabolism, including synthesis and degradation of proteins, is now considered as a desirable strategy for disrupting such undruggable proteins in cells. Small interfering RNA (siRNA) drug is one of the options to down-regulate the target protein abundance in human tissue. However, the currently available delivery system for siRNA to target tissue is limited[2].

The ubiquitin-proteasome system is a key mechanism of the regulated protein degradations in mammalian cells. The recent successes of proteasome inhibitors as the multiple myeloma drug proved the therapeutic potential of targeting the proteolysis[3]. More recently, clinically important myeloma drug lenalidomide and other immune-modulatory drugs (IMiDs) were reported to hijack cullin-4 RING ubiquitin

ligase by binding to the one of DDB and CUL4-associated proteins (DCAFs), cereblon (CRBN), to redirect the substrate selectivity of the ligase[4-7]. As a results of the reprograming of ubiquitin ligase activity, lenalidomide induces the proteasomal degradation of the transcription factors IKZF1, IKZF3 and casein kinase 1α in cells.

In Chapter II, I revealed the mechanism underlying anticancer activity of a series of sulfonamide derivatives, E7820, indisulam, and chloroquinoxaline sulfonamide (CQS)[8]. Based on the mass spectrometry-based proteomics, I demonstrated that anticancer sulfonamides induce protein complex assembly between U2AF related splicing factor, CAPERα, and an ubiquitin ligase, $CRL4^{DCAF15}$. This small chemical induced protein complex assembly results in selective ubiquitination and proteasomal degradation of the splicing factor to induce aberrant mRNA splicing and subsequent anti-proliferative effect in cancer cell lines. The molecular mechanism of these sulfonamides, in addition to that of IMiDs, suggests DCAFs are promising drug targets through the promotion of selective protein degradation (Figure I-1).

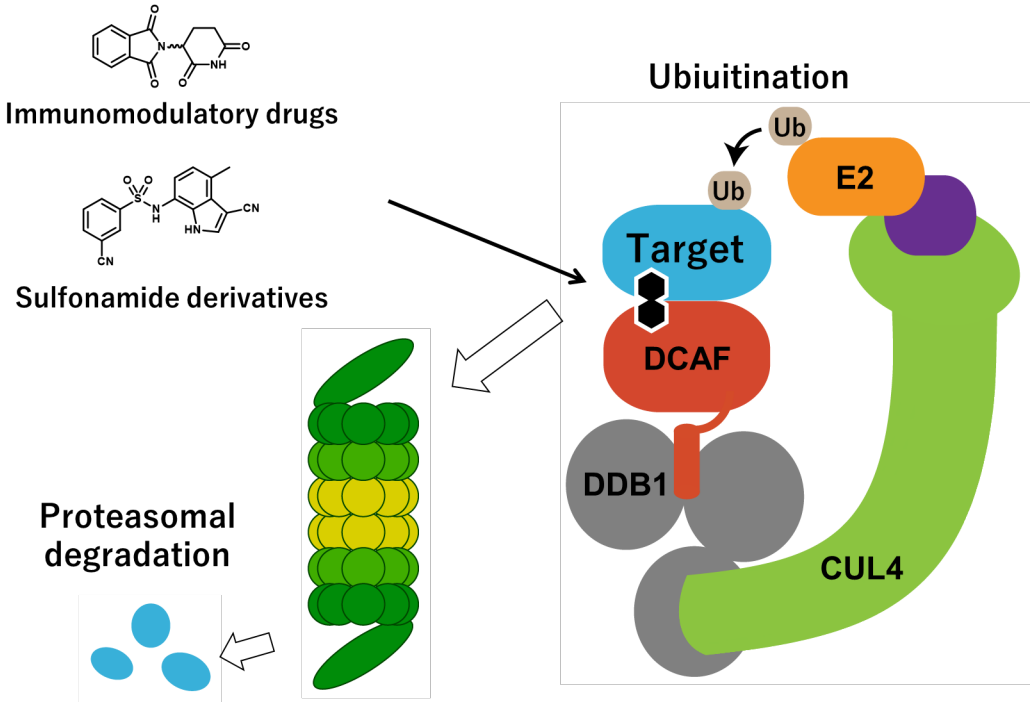

Figure I-1. Mechanism of the target protein degradation by the small chemicals. Immunomodulatory drugs (IMiDs) bind to one of DDB1 and CUL4-associated factors (DCAFs), CRBN. Binding of IMiDs reprograms the substrate selectivity of $CRL4^{CRBN}$ to induce ubiquitination of IKZF1, IKZF3, and CK1α. These ubiquitinated proteins are subsequently degraded by proteasome. Anticancer sulfonamide derivatives bind to DCAF15 to recruit and ubiquitinate the splicing factor CAPERα. Ubiquitinated CAPERα is also degraded by proteasome.

Chapter II

Selective Degradation of Splicing Factor CAPERα by Anticancer Sulfonamides

Summary

Target protein degradation is an emerging field in drug discovery and development. In particular, the substrate receptor proteins of the cullin ubiquitin ligase system play a key role in selective protein degradation, which is an essential component of the anti-myeloma activity of immunomodulatory drugs (IMiDs) represented by lenalidomide. Here, I demonstrate that a series of anticancer sulfonamides NSC 719239 (E7820), indisulam, and NSC 339004 (chloroquinoxaline sulfonamide, CQS) induce proteasomal degradation of an U2AF-related splicing factor, Coactivator of Activating Protein-1 and Estrogen Receptors (CAPERα) via $CRL4^{DCAF15}$ mediated ubiquitination in human cancer cell lines. Both CRISPR/Cas9-based knockout of DCAF15 and a single amino acid substitution of CAPERα conferred resistance against sulfonamide-induced CAPERα degradation and cell-growth inhibition. Thus, these sulfonamides represent selective chemical probes for disrupting CAPERα function and

designate DCAFs as promising drug targets for promoting selective protein degradation in cancer therapy.

Introduction

Protein metabolism, including protein ubiquitination and proteasomal degradation, has recently been discovered to be an important therapeutic modality for cancer. The proteasome inhibitor bortezomib has shown significant efficacy in the treatment of multiple myeloma, and the protein NEDDylation inhibitor MLN4924 is in clinical trials[3,9,10]. Furthermore, the myeloma drug lenalidomide (Figure II-1) was reported to target one of the DDB1- and CUL4-associated factors (DCAFs), cereblon (CRBN), and to induce selective degradation of the Ikaros family zinc finger proteins 1 and 3 (IKZF1 and IKZF3) and casein kinase 1α (CK1α) as key mechanisms of anticancer activity in multiple myeloma cells and the deletion 5q (del (5q)) subtype of myelodysplastic syndromes (MDS)[4-7,11-14]. CRBN and other DCAFs are components of the CUL4-RING ubiquitin ligase (CRL4) complex, and play a central role in substrate recognition for ubiquitination[15-17]. Furthermore, recent reports show that conjugation of the phthalimide moiety of thalidomide with a competitive antagonist of BET bromodomains induces the degradation of transcriptional coactivator BRD4 via $CRL4^{CRBN}$, suggesting that CRBN-based target protein degradation may also be

applicable to substrate proteins other than IKZF1 and IKZF3, and thus an accessible therapeutic strategy using chemical conjugation techniques[18-22].

Here, I initiated a target identification study for a series of anticancer sulfonamides NSC 719239 (E7820, **1**), indisulam (**2**), and NSC 339004 (chloroquinoxaline sulfonamide, CQS, **3**) (Figure II-1), based on observations that they may have clinical activity in cancer patients[23-25]. CQS and indisulam are chlorinated heterocyclic sulfonamide derivatives, and have unique mean-graph fingerprints in an NCI COMPARE analysis that are quite different from those of other anticancer drugs in clinical use (https://dtp.cancer.gov/databases_tools/compare.htm)[26], whereas E7820 has been shown to be a novel anticancer and anti-angiogenesis agent that inhibits VEGF- or FGF-2-induced tube formation of human umbilical endothelial cells (HUVEC)[27]. Although these sulfonamides have been the focus of drug discovery and development efforts over the past two decades, the primary target molecule and their precise mechanisms of action remain unclear[28-30]. I recently found that an indisulam-resistant clonal cancer cell line was cross-resistant to E7820 and CQS, but not doxorubicin and paclitaxel (Figure II-2)[28]. This suggests that the drug resistant mechanism is independent of P-glycoprotein-based multi-drug resistance (MDR) and associated with a mechanism of anticancer action which is common in these three sulfonamides.

In the present study, I report that E7820, indisulam, and CQS promote selective degradation of an U2AF-related splicing factor, Coactivator of Activating Protein-1 and Estrogen Receptors (CAPERα) by inducing protein complex assembly between CAPERα and $CRL4^{DCAF15}$. A single amino acid substitution of CAPERα conferred resistance against sulfonamide-induced CAPERα degradation and cell-growth inhibition, suggesting that CAPERα degradation is a key biochemical activity that underlies the anticancer properties of these compounds.

Results

Down-regulation of CAPERα by E7820, indisulam, and CQS

To clarify the cellular effect of E7820 at an early time point, I used a label-free quantitative proteome analysis strategy, Data-Independent Acquisition (DIA)[31]. In traditional Data-Dependent Acquisition (DDA) with a certain isobaric labeling technique, mass spectrometer randomly samples detectable peptides for fragmentation, often resulting in insufficient reproducibility. In DIA, all precursor ions are systematically fragmented with defined *m/z* windows, allowing highly reproducible quantification of peptides. Differential profiling of the cellular proteins in cells treated with E7820 and dimethyl sulfoxide (DMSO) demonstrated that there were significant decreases in CAPERα in both the human colon colorectal carcinoma cell line HCT116 and the human myelogenous leukemia cell line K562 6 hours after treatment with E7820 (Figure II-3a). *In vitro* staining of HCT116 cells showed that CAPERα co-localizes with SC35 in the nuclear speckle, as previously reported[32], and that there is a clear reduction in the CAPERα signal following E7820 treatment (Figure II-3b). I then compared the effects of E7820, indisulam, and CQS on CAPERα protein expression by performing immunoblot analysis to confirm the reduction of CAPERα is a common biochemical consequence among these molecules. There was a good correlation between the extent of CAPERα reduction and cell-growth inhibition for all

three sulfonamides (Figure II-3c, Table 1). A quantitative polymerase chain reaction (qPCR) assay further demonstrated that the mRNA expression of *CAPERα* increased following the protein reduction in both HCT116 and K562 cells (Figure II-3d, 3e), suggesting protein down-regulation by these sulfonamides is posttranscriptional and the gene expression of *CAPERα* may be negatively regulated by CAPERα protein.

CAPERα degradation depends on CRL4^{DCAF15}

To examine whether this sulfonamide-induced CAPERα reduction is dependent on cullin-RING ubiquitin ligase (CRL), I assessed the effect of MLN4924, a small molecule inhibitor of NEDD8-activating enzyme (NAE), on protein reduction, since CRL activity depends on NEDDylation[9]. I found that MNL4924 completely blocked E7820-induced reduction of CAPERα, as did the myeloma drug bortezomib, a selective proteasome inhibitor (Figure II-4a), indicating that E7820 induces CRL-mediated ubiquitination and proteasomal degradation of CAPERα. Therefore, I hypothesized that these sulfonamides induce a protein-protein interaction between CAPERα and the CRL complex.

To identify the binding partner of CAPERα, I used CAPERα immunoprecipitation followed by DIA. Differential proteome analysis demonstrated

that E7820 enhances the ability of CAPERα to bind to DCAF15 and DDB1 in both HCT116 and K562 cells (Figure II-4b). DDB1 functions as a linker between the CUL4 scaffolds and DCAF substrate receptors to build the CRL4 complexes, which regulate diverse protein ubiquitination and cellular functions[16,17]. To confirm whether DCAF15-DDB1 plays a key role in CAPERα degradation, I performed a siRNA-mediated knockdown of *DCAF15* and *DDB1* in HCT116 cells. As expected, both *DCAF15* and *DDB1* knockdowns rescued sulfonamide-induced CAPERα degradation and inhibition of cell growth in HCT116 cells (Figure II-5). Since DDB1 functions as a general linker protein in the CRL4 complex, I suspected that DCAF15 might be a more suitable protein target for compound mediated selective protein degradation. Therefore, I established a *DCAF15* knockout clone of HCT116 using CRISPR/Cas9-based gene editing (Figure II-6). An immunoblot analysis and cell viability assay revealed that *DCAF15*-/- HCT116 cells were also resistant to sulfonamide-induced CAPERα degradation and cell-growth inhibition in spite of strong growth inhibition by other cytotoxic agents (Figure II-7, Figure II-8). Unfortunately, I was unable to identify the cullin protein(s) because there were insufficient differences between compound-induced interactions and non-specific binding of cullin protein under these immunoprecipitation conditions. Therefore, I next assessed the effect of

CUL4A and/or *CUL4B* knockdown on CAPERα degradation. Interestingly, the double knockdown of *CUL4A* and *CUL4B* significantly prevented E7820-induced CAPERα degradation, whereas the single knockdown of either *CUL4A* or *CUL4B* did not (Figure II-9), indicating that CUL4A and CUL4B may be involved in DCAF15-DDB1-mediated protein ubiquitination in a redundant manner[17,33].

DCAF15 is the primary target of anticancer sulfonamides

The stable transfection of *DCAF15* into *DCAF15*-/- HCT116 clonal cells successfully restored the E7820-induced protein degradation (Figure II-10a). Therefore, I examined the identity of the molecular complex that includes E7820, CAPERα, DCAF15, and DDB1 using *DCAF15*- or mock-vector-transfected *DCAF15*-/- HCT116 cells. Immunoprecipitation with the anti-CAPERα antibody followed by immunoblot analysis confirmed that E7820 induces protein complex assembly between CAPERα and DCAF15-DDB1. The antibody did not pull down DDB1 in the mock-transfected cells but did in the *DCAF15*-transfected cells following E7820 treatment, indicating that DDB1 binds to CAPERα via DCAF15 (Figure II-10b). In addition, CAPERα immunoprecipitation followed by an ubiquitin immunoblot analysis confirmed that E7820-induced CAPERα ubiquitination is dependent on DCAF15 (Figure II-10C). Next,

I immunoprecipitated CAPERα from tritium-labeled E7820 (^{3}H-E7820, **4**, Figure II-1) treated HCT116 cells with or without cold E7820 competition. The anti-CAPERα antibody captured a strong tritium count from the *DCAF15*-transfected cells, but not from the mock-transfected or cold E7820 competed cells, indicating that the E7820 molecule is present in the CAPERα-DCAF15-DDB1 complex (Figure II-10d). To identify a direct binding partner for E7820, I performed photo-affinity labeling with a biotinylated photoactive E7820 probe (**5**, Figure II-1). Photo-affinity labeling followed by biotin-streptavidin affinity purification selectively captured and enriched DCAF15, with E7820, indisulam, and CQS all competing for probe binding to DCAF15 (Figure II-10e). Together, these findings demonstrate that these three sulfonamides induce protein complex assembly between CAPERα and $CRL4^{DCAF15}$, thereby promoting ubiquitination and proteasomal degradation of CAPERα. Moreover, the deleterious effect of *DCAF15* knockdown on HCT116 cell growth indicates that the anti-proliferative activities of these sulfonamides are not caused by simple antagonism toward DCAF15 (Figure II-5c).

The biochemical activity of these sulfonamides might be similar to that of lenalidomide[5,6]. Therefore, I assessed the cross-reactivity of small-molecule-mediated protein degradation between E7820 and lenalidomide in the multiple myeloma cell line

MM.1S. E7820 treatment resulted in the clear degradation of CAPERα but did not affect the expression of IKZF1 or IKZF3 in the MM.1S cells. By contrast, lenalidomide did not decrease CAPERα expression at a concentration of 10 μM, which is sufficient for IKZF1 and IKZF3 degradation (Figure II-11). These results verify the specific protein degradations of E7820 and lenalidomide are independent and not cross-reactive.

CAPERα degradation is crucial for anticancer activity

I also performed differential exome sequencing of parental HCT116 cells and sulfonamide-resistant clonal cells established by serial exposure to a drug concentration escalation procedure (Figure II-2)[28]. Exome sequencing detected 17 differential gene mutations in the sulfonamide-resistant cells, including a heterozygous G268V/missense mutation in *CAPERα* and a heterozygous R87* nonsense mutation (Figure II-12, Table 2). To investigate the mutational status of the CAPERα protein in the sulfonamide-resistant cells, I analyzed immunoprecipitated CAPERα using liquid chromatography-tandem mass spectrometry (LC-MS/MS), which demonstrated that the G268V mutant CAPERα was dominantly expressed in resistant cells (Figure II-13). I also found that E7820 did not degrade CAPERα in the resistant cells (Figure II-14) and did not enhance the protein-protein interaction between DCAF15/DDB1 and CAPERα

(Figure II-15). Therefore, I hypothesized that the G268V mutation confers resistance to E7820-induced CAPERα degradation and cell-growth inhibition. To test this hypothesis, I used CRISPR/Cas9-based gene editing to establish CAPERα-G268V mutant cells, which were then treated with E7820. As expected, gene sequencing revealed that the E7820 treatment enriched the G268V mutant cells in all transfectants (Figure 16). Therefore, I performed cell cloning and selected clonal cells which have heterozygous CAPERα-G268V mutations for further investigation (Figure II-16). Immunoblot analysis showed that these K562-G268V mutant cells exhibited sulfonamide-induced incomplete degradation of CAPERα (Figure II-17). Notably, an immunoprecipitation-LC-MS/MS analysis of CAPERα demonstrated that both wild type and G268 mutant CAPERα proteins are co-expressed in K562-G268V mutant cells, and that only the wild type protein is degraded by E7820, resulting in the retention of the mutant protein (Figure II-18). The nuclear magnetic resonance (NMR)-based solution structure of the CAPERα RNA recognition motif 2 (RRM2) domain reported in Protein Data Base (PDB 2JRS) shows that ^{268}glycine is located in the alpha-helix and directed outside the protein (Figure II-19). Combined, this structure model and my data suggest that ^{268}glycine may be a part of degron of these sulfonamides and DCAF15 protein complex.

A cell-growth-inhibition assay indicated that the G268V mutation in *CAPERα* confers resistance to the anti-proliferative activity of these sulfonamides in spite of strong growth inhibition by other cytotoxic agents (Figure II-20). Compared to sulfonamide-resistant HCT116 cells, K562-G268V cells were more sensitive to these sulfonamides, which might be due to heterozygous gene editing in K562 cells. In addition, siRNA-mediated *CAPERα* knockdown resulted in significant growth inhibition not only in the parental HCT116 cells but also in the resistant clonal cells (Figure II-21). All of these findings indicate that CAPERα has a critical biological function in HCT116 cell viability and the haploinsufficiency of HCT116 may render them particularly sensitive to E7820, indisulam, and CQS.

CAPERα is an U2AF-related splicing factor (also designated RBM39, HCC1, FSAP59, and RNPC2) that serves as a coactivator for the transcription factors AP1, ERα, ERβ, ERRα, and NF-κB, and is involved in nuclear receptor-dependent alternative splicing[32,34-38]. It has previously been reported that RNAi-mediated knockdown of *CAPERα* changes the splice-form of vascular endothelial growth factor A (VEGF-A)[35,36,38]. Here, I confirmed the modulation of VEGF-A alternative splicing via the small-molecule-induced knockdown of the CAPERα protein in HCT116 cells using exon junction targeted qPCR. In particular, I observed a significant decrease in

VEGF-A-189 and a concomitant increase in VEGF-A-121 following treatment with these sulfonamides or *CAPERα* siRNA (Figure II-22). I also undertook a comprehensive comparison of the siRNA-based genetic perturbation of *CAPERα* and the small-molecule-based chemical perturbation of the protein using microarray-based transcriptomic analysis (Figure II-23a) and confirmatory qPCR analysis (Figure II-23b), which showed that there was a high correlation ($r^2 = 0.649$) between the *CAPERα* siRNA (20 nM, 48 hours) and E7820 (1 μM, 24 h) treatments. In the qPCR assay, cells treated with these sulfonamides or siRNA exhibited changes in gene expression, with two genes upregulated (*RBM15* and *ZNF177*) and four downregulated (*ITGA2*, *SLC7A11*, *GSS*, and *CCNH*) (Figure II-23b).

Discussion

In this study, I clarify that the anticancer action of the small molecule sulfonamides E7820, indisulam, and CQS is primarily driven by assembly of protein complex between CAPERα and DCAF15, which results in selective ubiquitination and degradation of CAPERα via $CRL4^{DCAF15}$. The binding mode among the compound and proteins has yet to be fully elucidated, and in particular additional molecule(s), not identified in this study, might mediate the compound-proteins complex assembly.

However, this molecular mechanism would appear to closely resemble the lenalidomide-promoted CRBN-dependent destruction of IKZF1 and IKZF3, which results in anti-myeloma activity in the clinic. My finding, in addition to the lenalidomide story, suggests that the ubiquitin ligase system-targeted drug discovery and development may be expanded through the identification of different substrate protein targets to be coupled with specific DCAFs by small molecule like IMiDs and the present anticancer sulfonamides. Therefore, the structural basis of sulfonamide-induced degron recognition by $CRL4^{DCAF15}$ should be clarified in future. In addition, $CRL4^{DCAF15}$ might have other substrates which were not detected in my limited proteome datasets. Further investigations with these sulfonamides as selective chemical probes may extend my understanding of the biological functions of CAPERα, guiding us to the selection of right target cancer types with enhanced sensitivity to these drugs, e.g., cancers with aberrant splicing that is linked to malignant transformation of cells and disease progression[39].

Significantly, the putative mode of action of these sulfonamides, acting as a 'molecular glue', raises an implication that DCAF-dependent, small molecule ligand-induced selective protein degradation might be originated in natural phenomenon which can be promoted by primary or secondary metabolites, as exemplified by the

plant hormone auxin (Figure II-1). Auxin connects SCF^{TIR1} ubiquitin ligase and Aux/IAA transcriptional repressors to regulate the growth and behavioral processes of plants[40]. Thus, my observation here might recapitulate a pharmacological example of processes that have already occurred in nature, suggesting new therapeutic possibilities through strategic chemical and pharmacologic intervention in such protein homeostasis pathways.

Materials and Methods

Reagents.

E7820 (99.82% purity) and indisulam (E7070, 99.80% purity) were manufactured by Eisai Co. Ltd.; bortezomib, MLN4924, PR-619, and lenalidomide were purchased from LC Laboratories, Focus Biomolecules, Abcam, and BePharm Ltd., respectively; and doxorubicin and paclitaxel were purchased from Wako. All compounds were dissolved in DMSO.

Cell culture.

HCT116 and MM.1S cells were obtained from the American Type Culture Collection (ATCC); and K562 cells were obtained from the Health Science Research Resources Bank (HSRRB). Cells were cultured in RPMI-1640 (Wako) supplemented with 10% fetal bovine serum (FBS; Sigma Aldrich) and 1% penicillin-streptomycin (Wako), and grown at 37 °C in a humidified incubator under 5% CO_2. All cell lines had been authenticated by STR profiling, and confirmed mycoplasma free. Cells were treated with compounds dissolved in DMSO, and the equal amount of DMSO was added to control cells. DMSO concentrations were under 0.2%.

Cell lysis and tryptic digestion for LC-MS/MS analysis.

HCT116 or K562 cells were plated in 10-cm inner diameter (ID) dishes and cultured for 2 days before being treated with either DMSO or 3 μM of E7820 for 6 hours. The HCT116 cells were washed twice with cold phosphate buffered saline (PBS, Wako), lysed using 7 M UREA (Wako), 2 M Thio-UREA (Wako), 3% 3-[(3-cholamidopropyl)dimethylammonio]-1-propanesulfonate (CHAPS, Pierce), 50 mM NH_4HCO_3 (Wako), 50 mM dithiothreitol (DTT; Pierce or Calbiochem), and cOmplete(R) Protease Inhibitor Cocktail (Roche), and scraped onto the culture dish. The K562 cell cultures were collected and centrifuged to remove the supernatant, and the cells washed with cold PBS, centrifuged, and lysed using the same buffer as for the HCT116 cells. After removing cellular debris by centrifugation, the total protein contents were analyzed using Pierce 660 nm Protein Assay reagent.

The protein alkylation and digestion procedure followed the Filter Aided Sample Preparation (FASP) method[41], with some modification. Cell lysates of 100 μg protein were loaded on a Nanosep(R) 10K filter unit (PALL) and centrifuged at 12000 × *g* for 20 min at rt. The protein samples on the filter unit were washed with an 8 M UREA/50 mM NH_4HCO_3 solution, and carbamidomethylated with 50 mM of iodoacetamide for 20 min at rt in the dark. The iodoacetamide solutions were then removed by centrifugation and the samples were washed with an 8 M UREA / 50 mM NH_4HCO_3

solution three times. The proteins were dissolved in a 5 M UREA / 50 mM NH_4HCO_3 solution and then digested in the filter unit by 1 μg Lys-C (Wako) at 37 °C for 1 hour. The samples were then diluted four-fold with 50 mM NH_4HCO_3 solution to make 1 M UREA sample solutions, which were passed through a second digestion step using 1 μg sequencing grade trypsin (Promega) at 37 °C overnight. The digested samples were collected from the filter unit by centrifugation, following which the filters were washed twice with 8 M UREA. The samples were then acidified to make approximately 1% trifluoroacetic acid (TFA; Pierce) and desalted on an Empore solid phase extraction cartridge (C18 standard density, 3M). Peptides were eluted from the column with 80% acetonitrile/1% TFA, and then dried in a SpeedVac concentrator (Thermo Fisher Scientific).

LC-MS/MS analysis.

Tryptic peptides from the whole cell lysate or immunoprecipitation samples were reconstituted in 5% methanol/0.1% TFA and analyzed in a nano-flow LC-MS/MS system using a Q Exactive™ HF mass spectrometer (Thermo Fisher Scientific) coupled with an online UltiMate(R) 3000 Rapid Separation LC (RSLC, Dionex) and an HTC PAL sample injector (CTC Analytics, Zwingen, Switzerland) fitted with a

microcapillary column (360 nm outer diameter (OD) × 100 μm ID), which was packed with < 20 cm of ReproSil C18-AQ 5 μm beads (Dr. Maisch GmbH) and equipped with an integrated electrospray emitter tip (P-2000 laser-based puller; Sutter Instruments). Each sample was loaded onto the capillary column by 4 μL full-loop mode injection. For LC separation, a mobile phase A of 4% acetonitrile/0.5% acetic acid (Wako) and a mobile phase B of 80% acetonitrile/0.5% acetic acid were used for multiple linear gradient elution from 1–37% of B over 60 min, 37–67% of B over 10 min, 67–99% of B over 5 min, and then held at 99% of B for 10 min, at 500 nL/min. The total analysis time for each sample was 120 min.

Each sample was analyzed twice using two different acquisition modes of the Q Exactive HF mass spectrometer. The first of these was Data-Dependent Acquisition (DDA), which used higher energy collision dissociation (HCD) MS/MS scans (resolution 30,000) for the top 15 most abundant ions of each full-scan MS from *m/z* 350 to 1500 (resolution 60,000) with a full-scan MS ion target of 3×10^6 ions and an MS/MS ion target of 2×10^5 ions. The maximum ion injection time for the MS/MS scans was 100 msec, the HCD normalized collision energy was set to 27, the dynamic exclusion time was set to 20 sec, and the peptide match and isotope exclusion functions were enabled. The second mode was Data-Independent Acquisition (DIA), which

consisted of 30 HCD MS/MS scans (resolution 30,000) with an isolation window of 27 Da (25 Da step) to cover *m/z* 350 to 1100 and a full scan MS from 350 to 1100. This used a full scan MS ion target of 3×10^6 ions and an MS/MS ion target of 1×10^6 ions. The maximum ion injection time for the MS/MS scans and the HCD normalized collision energy were the same as for DDA.

LC-MS data analysis.

All DDA mass spectra were analyzed with Proteome Discoverer ver. 1.4 (Thermo Fisher Scientific) using a human Swiss-Prot database. Both MASCOT and SEQUEST-HT algorithms were used for MS/MS searching of the proteome datasets, with the following parameters: oxidation of methionine and protein *N*-terminal acetylation as variable modifications; carbamidomethylation of cysteine as a fixed modification; trypsin as the digestion enzyme; two missed cleavages per peptide were allowed; the mass tolerance for precursor ions was set to 10 ppm; and the mass tolerance for product ions was set to 20 mDa. A maximum false discovery rate (FDR) of 1% was applied for peptide identification. Protein identification required more than two peptides per protein without protein grouping.

For the DIA dataset, peptide ion peak areas were extracted and integrated using Skyline software ver. 3.1.0.7382[42]. Peptide spectral libraries were established based on Thermo's MSF files using Proteome Discoverer ver. 1.4 with a cutoff score of 0.99. The target peptide was allowed to include the following structural modifications: oxidation of methionine and protein *N*-terminal acetylation as variable modifications; carbamidomethylation of cysteine as a fixed modification; and a maximum of two missed cleavages. Transitions were set with the following conditions: precursor charges-2, 3, 4; ion charges-1, 2; ion types-y, p; product ions-pick three product ions from the precursor *m/z* to the last ion, excluding the DIA precursor window; auto-select all matching transitions. Peak areas with a maximum of seven peptides per protein were extracted from the scans within 1 min of MS/MS identification. The product ion peak areas were then summed to yield the peptide peak area, which was used for statistical analysis. The $\log_2$ fold change in each peptide following E7820 treatment relative to the control value (DMSO treatment) was assessed using Welch's t-test ($p<0.05$) in Excel 2010 (Microsoft).

Antibodies.

The following antibodies were used: anti-CAPERα mouse monoclonal antibody (Santa Cruz Biotechnology, Inc, G-10; for immunoblot, 1:1000 dilution), anti-CAPERα rabbit polyclonal antibody (Bethyl Laboratories, A300-291A; for immunostaining and immunoprecipitation), anti-DCAF15 goat polyclonal antibody (Santa Cruz Biotechnology, Inc, N-16; 1:400 dilution), anti-DDB1 rabbit polyclonal antibody (Bethyl Laboratories, A300-462A; 1:2000 dilution), anti-ubiquitinylated proteins mouse monoclonal antibody FK2 (HRP conjugated, Enzo Life Sciences; 1:1000 dilution), anti-Ikaros (IKZF1) rabbit polyclonal antibody (Cell signaling Technologies, #5443; 1:1000 dilution), anti-Aiolos (IKZF3) rabbit polyclonal antibody (Novus Biologicals, NBP2-24495; 1:1000 dilution), anti-GAPDH rabbit polyclonal antibody (Cell Signaling Technologies, 14C10; 1:2000 dilution), anti-vinculin mouse monoclonal antibody (Abcam, SPM227; 1:2000 dilution), normal rabbit IgG (Wako, 148-09551; for immunoprecipitation), horse anti-mouse IgG HRP conjugated antibody (Cell signaling Technologies, #7076; 1:2000 dilution), goat anti-rabbit IgG HRP conjugated antibody (Cell Signaling Technologies, #7074; 1:2000 dilution), and donkey anti-goat IgG HRP conjugated antibody (Santa Cruz Biotechnology, Inc., sc-2020; 1:4000 dilution).

Cell immunostaining.

The cells were washed with PBS and fixed in 2% paraformaldehyde (Wako) for 30 min. The cells were then rewashed with PBS, and permeabilized using 0.1% Triton X-100 for 30 min and blocked with Block Ace (DS Pharma Biomedical). The cells were incubated with anti-CAPERα antibody (1:2000 dilution; Bethyl Laboratories) and anti-SC-35 antibody (1:400 dilution; BD) overnight, washed with 0.05% tween20 / Tris-buffered saline (TBS), and then labeled with Cy5-conjugated anti-rabbit IgG antibody (Invitrogen), AlexaFluor488-conjugated anti-mouse IgG antibody (Invitrogen), and Hoechst 33342 (Sigma). Image acquisition was performed using CellVoyager6000 (CV6000), which is an automated high-throughput cytological discovery system with laser-scanning confocal microscopes and image analysis software (Yokogawa Electric Corp., Tokyo, Japan). Three channels of excitation laser wavelengths were used (405, 488, and 635 nm) and each well was scanned with a 40 × objective to produce an image.

Immunoblot analysis.

The cells were washed with PBS and lysed with cold Pierce RIPA buffer (Thermo Fisher Scientific) containing the cOmplete(R) Protease Inhibitor Cocktail (Roche). After removing the cell debris by centrifugation, the total protein contents

were analyzed using the Pierce BCA assay. The extracts were reduced by DTT (Pierce) and separated on 4–20% SDS-polyacrylamide gradient gels (Biorad), following which the proteins were transferred to a nitrocellulose membrane (GE Healthcare Life Science) or PVDF (Biorad) membrane by electroblotting. After blocking with TBS (Takara) containing 5% non-fat dry milk (Wako) and 0.1% Tween-20 (Wako), the membrane was incubated with primary antibodies, followed by horseradish peroxide-conjugated secondary antibodies. Immunodetection was performed using Amersham ECL Prime (GE Healthcare Life Science), and a lumino-image analyzer (LAS-4000; GE Healthcare Life Science).

The DCAF15 immunoblot required some specific conditions. The cells were lysed with 4% SDS / 50 mM Tris-HCl (pH 7.5) containing the cOmplete(R) Protease Inhibitor Cocktail (Roche). After being reduced by DTT (Pierce), the protein samples were alkylated using iodoacetamide (Wako) to block non-specific binding by the antibody. The Biorad Trans-Blot(R) Turbo system was used for electroblotting. After blocking with TBS (Takara) containing 5% non-fat dry milk (Wako) and 0.1% Tween-20 (Wako), the membrane was incubated with the primary antibody anti-DCAF15 (N-16; Santacruz) in Canget Signal 1(R) (Toyobo Life Science

Department) at 4 °C overnight. Canget Signal 2(R) was also used for the second antibody incubation.

Co-immunoprecipitation of CAPERα.

Cells were plated in 10-cm ID dishes at a density of 2×10^6 cells and incubated for 2 days. The cells were then pretreated with bortezomib for 30 min, following which E7820 or DMSO was added. After 3 hours' incubation, the cells were washed twice with cold PBS and lysed with 0.25 M sucrose (Wako) / 0.3 mM sodium diethyldithiocarbamate trihydrate (Wako) / 1 mM $CaCl_2$ (Wako) / 1 mM $MgCl_2$ (Wako) / 0.5 uM $FeCl_3$ (Merck) / 0.1% PBS / 25 mM Tris-HCl (pH 7.5) (Nippongene) / cOmplete Protease Inhibitor Cocktail EDTA-free (Roche) lysis buffer in a culture dish. The cell lysates were collected and sonicated using an Astrason Ultrasonic Processor (MISONIX) and centrifuged at 12,000 × *g* for 20 min at 4 °C to remove any insoluble material. Protein A/G agarose beads (Pierce) and the anti-CAPERα antibody were incubated in lysis buffer at 4 °C, and then added to the cell lysates and incubated overnight at 4 °C in an end over end shaker. Following incubation, the samples were centrifuged at 2000 × *g* for 1 min at 4 °C to remove the supernatant, and the beads were then washed with sucrose buffer three times. The washed beads were extracted using 8

M UREA / 50 mM NH_4HCO_3 / 50 mM DTT solution followed by the FASP protocol described in the previous section. For immunoblotting, the beads were extracted using 10% SDS/gel loading buffer (Biorad) / 50 mM DTT (Pierce).

Cell-based ubiquitination assay.

DCAF15- or mock-vector-transfected *DCAF15*-/- HCT116 cells were plated in 10-cm ID dishes at a density of 2×10^6 cells and incubated for 2 days. The cells were then pretreated with bortezomib for 30 min, following which PR-619 (30 μM) and either DMSO or E7820 (3 μM) were added. After 3 hours' incubation, the cells were washed twice with cold PBS and lysed in 1 mL of cold Pierce RIPA buffer containing the cOmplete(R) Protease Inhibitor Cocktail and PR-619 (30 μM). The cell lysates were then sonicated in an ice-cold bath and frozen at −80 °C. The thawed cell lysates were again sonicated in an ice-cold bath and centrifuged at 12000 × *g* for 20 min at 4 °C to remove any insoluble material. Protein A/G agarose beads (Pierce) and anti-CAPERα antibody were incubated in 0.25 M sucrose-based buffer at 4 °C, and were then added to the cell lysates and incubated at 4 °C overnight in an end over end shaker. Following incubation, the beads were centrifuged at 2000 × *g* for 1 min at 4 °C to remove the supernatant, and were then washed with RIPA buffer containing protease inhibitor and

PR-619 three times. The washed beads were extracted using 10% SDS / gel loading buffer (Biorad) / 50 mM DTT (Pierce) for immunoblotting.

^{3}H-E7820 pulldown assay.

DCAF15- or mock-vector-transfected *DCAF15*-/- HCT116 cells were plated in 10-cm ID dishes at a density of 2×10^{6} cells per dish and incubated for 2 days. The cells were then pretreated with bortezomib for 30 min, following which ^{3}H-E7820 (final 1 μM) with or without cold E7820 (final 20 μM) were added. After 3 hours' incubation, cell lysis and immunoprecipitation with the anti-CAPERα antibody were performed using the same method as described in the previous co-immunoprecipitation section. The washed beads were extracted by boiling them in 100 μL of sodium dodecyl sulfate polyacrylamide gel electrophoresis (SDS-PAGE) sample buffer at 95 °C for 5 min. Half of each sample solution (50 μL) was diluted with 15 mL of Hionic-Fluor (PerkinElmer) and then analyzed twice using a liquid scintillation counter (PerkinElmer Tri-Carb2100TR).

Photo-affinity labeling using the biotinyl photoactive E7820 probe.

DCAF15-vector-transfected *DCAF15*-/- HCT116 cells were plated in 10-cm ID dishes at a density of 2.5×10^6 cells and incubated for 2 days. Following incubation, the cells were washed twice with cold PBS and lysed with 0.25 M sucrose / 0.3 mM sodium diethyldithiocarbamate trihydrate / 1 mM $CaCl_2$ / 1mM $MgCl_2$ / 0.5 uM $FeCl_3$ / 0.1% PBS / 25 mM Tris-HCl (pH 7.5) / cOmplete(R) Protease Inhibitor Cocktail EDTA-free (Roche) lysis buffer in a culture dish. The cell lysates were collected and sonicated using an Astrason Ultrasonic Processor (MISONIX), and were then centrifuged at 12,000 × *g* for 20 min at 4 °C to remove any insoluble material. The biotinyl photoactive E7820 probe (0.5 μM) was added to the cell lysates with a competitor (E7820, indisulam or CQS (30 M each), or DMSO) and then incubated for 30 min at 4 °C in an end over end shaker. Following incubation, the samples were irradiated with ultraviolet (UV) light for 30 seconds using a 365-nm cut filter, and then 10% SDS solution (final about 1%) was added. Streptavidin beads that had previously been washed were added to the sample and incubated for 2 hours at rt in an end over end shaker. The streptavidin beads were then collected by centrifugation and washed with a 0.5 % SDS / 50 mM Tris-HCl (pH 7.5) solution four times. The washed beads were extracted using 10% SDS/SDS-PAGE sample buffer / 50 mM DTT / 20 mM biotin for immunoblot analysis.

Quantitative RT-PCR.

TaqMan Gene Expression Assays (Life Technologies) used in this study are summarized in Supplementary Table 3.

For time course analysis of *CAPERα* gene expression and confirmation of siRNA-mediated knockdown, total RNA extraction and cDNA synthesis were performed using the Cell-to-CT™ kit (Ambion), according to the manufacturer's protocol. A quantitative PCR analysis of the cDNA (total RNA equivalent) was carried out in duplicate (n = 3 biological replicates) using the TaqMan(R) Fast Advanced Master Mix (Life Technologies) on a ViiA7 Real-time PCR System (Life Technologies). Cycle threshold (Ct) values were determined using ViiA7 software version 1.1 (Life Technologies). The relative gene expression normalized against the expression level of GAPDH was calculated using Excel 2010 (Microsoft).

For analysis of the VEGFA splicing variant and a putative pharmacodynamic marker of CAPERα reduction, total RNA was prepared from HCT116 cells using RNeasy mini spin columns (Qiagen), according to the manufacturer's protocol. The yield and quality of each isolated total RNA sample was determined using a NanoDrop(R) 1000 spectrophotometer (Thermo Fisher Scientific). The cDNA synthesis

was performed using a High Capacity cDNA Reverse Transcription Kit with RNase Inhibitor (Life Technologies), according to the manufacturer's instructions. Quantitative PCR analysis of the cDNA (total RNA equivalent) was carried out in duplicate (n = 3 biological replicates) using the TaqMan Gene Expression Master Mix (Life Technologies) on an ABI7900HT Real-time PCR System (Life Technologies). Cycle threshold (Ct) values were determined using SDS software version 2.2 (Life Technologies). A six-point standard curve was used to determine the PCR efficiency and relative quantitation. The relative gene expression normalized against the expression level of GAPDH was calculated using Excel 2010 (Microsoft).

Reverse transfection of siRNA.

ON-TARGETplus siRNA and DharmaFECT 2 transfection reagent were obtained from GE Dharmacon. The siRNA used in this study are summarized in Supplementary Table 4.

For siRNA-mediated knockdown in HCT116 cells, 5 μL of DharmaFECT 2 transfection reagent and 10 μL of 20 μM siRNA solution were mixed separately with 375 μL Opti-MEM serum-free medium. After 5 min incubation at rt, these two solutions were mixed and incubated for more than 20 min at rt to generate a

siRNA/DharmaFECT complex. Following incubation, 15 μL or 375 μL aliquots of the siRNA/DharmaFECT complex were added into wells of a 96-well plate or 6-well plate, respectively. Trypsinized HCT116 cells in antibiotic-free medium were then added to each well to give a final concentration of 20 nM siRNA. The cells were incubated at 37 °C in 5% CO_2.

The knockdown efficacies of siRNA were assessed using qPCR or immunoblot analyses. J-011965-06 (RBM39), J-031237-18 (DCAF15), and J-012890-07 (DDB1) were then selected for further knockdown experiments.

Plasmids for CRISPR/Cas9-based genome editing[43,44].

The plasmid pC3-vector was constructed by deleting the SV40-Neo-pA module from the pcDNA3.1 vector (Thermo Fisher Scientific) using PCR-based mutagenesis (PrimeSTAR MAX DNA Polymerase; Clontech Laboratories Inc.). The DNA fragment coding hSpCas9-NLS was synthesized with codon-optimization by the GeneArt(R) gene synthesis service (Thermo), and fused with the DNA fragments that code the T2A peptide sequence and the green fluorescent protein hmAzamiGreen (Amalgaam Co., Ltd.). To construct the Cas9 expression plasmid pC3-hCas9N-2A-hmAG, hSpCas9-NLS and 2A-hmAzamiGreen were subcloned into

the pC3-vector. To guide RNA expression, the pMA-U6-BbsI vector was constructed. The DNA sequence of the U6 promoter-BbsI-sgRNA scaffold module was custom synthesized and subcloned into the pMA-vector by GeneArt service (Thermo). Oligonucleotides for the target sequence were synthesized, annealed, and subcloned into the BbsI site of the pMA-U6-BbsI vector.

Plasmids for DCAF15 expression.

The piggyBac transposon vector pPBef1-mcs was constructed from the PB-EF1-MCS-IRES-GFP Vector PB530A-2 (System Biosciences Inc.) by removing 1.4 kb of the EcoRI-SalI fragment, which codes IRES-copGFP. The DCAF15 open reading frame (ORF) (NCBI Reference Sequence: NM_138353) was synthesized by GeneScript. The IAG2AP module containing the IRES sequence followed by DNA encoding the hmAzamiGreen-T2A-Puromycin resistant gene was constructed using the In-Fusion method (Clontech). The EuRed ORF, which encodes the red fluorescence FusionRed protein (Evrogen) with codon modification, was synthesized by GeneArt service (Thermo). pPBef1-DCAF15-IAG2AP and the control plasmid PBef1-EuRed-IAG2AP were constructed by connecting each module using the In-Fusion method.

Transfection.

HCT116 or K562 cells were seeded at a density of 5.0×10^5 cells per well in a six-well plate before being transfected with plasmids using Lipofectamine(R) 3000 reagent (Thermo) the following day. Approximately 250 μL of the transfection mixture contained 2.5–3.0 μg of plasmid DNA, 7.5 μL of Lipofectamine 3000, 5.0 μL of P3000 solution, and 250 μL OptiMEM (Thermo).

For the knockout of DCAF15, 1.0 μg of the Cas9-plasmid and 1.0 μg of the sgRNA-plasmid (sgRNA sequence: CTCCAGCACATAGTACAGCTTGG, where the underlined 3-bp sequence is a Protospacer Adjacent Motif (PAM) sequence) were co-transfected into HCT116 cells. At 46 hours after transfection, the transfected cells were dissociated using Trypsin-EDTA solution (Wako) and mixed with the growth medium. The resuspended cells were filtered using a strainer cap tube and several hundred hmAzamiGreen positive cells were collected with a SONY SH800Z cell sorter. Following cell sorting, the transfected cells were treated and selected using 1 μM E7820, and were then cloned to establish *DCAF15-/-* HCT116 clonal cells. Knockout of the *DCAF15* gene was confirmed by amplicon sequencing, as described below.

For point-mutation introduction, 1.0 μg of the Cas9-plasmid, 1.0 μg of the sgRNA-plasmid (sgRNA sequence: TAACTGAAGATATGCTTCGTGGG, where the

underlined 3-bp sequence is a Protospacer Adjacent Motif (PAM) sequence), and 1.0 μg of antisense donor-ssDNA (GAAGATTCATTGAAGAACCTGGACTTACTCTTCCAAAAGGCTCAAAGATAACACGAAGCATATCTTCAGTTATGTTGAAGTGTAATGAGCCCACATAAA, where the underlined 3-bp sequence represents the G268V mutation site) were co-transfected into K562 cells. The transfected cells were treated and selected using 1 μM E7820, and were then cloned to establish K562-G268V clonal cells. Introduction of the mutation was confirmed by amplicon sequencing for the genomic DNA (see below) and by immunoprecipitation/LC-MS/MS analysis for the protein.

For DCAF15 expression, following the transfection of HCT116 cells with DCAF15 and a mock vector using the piggyBac system with Lipofectamine 3000, the cells were treated and selected using 1 mg/mL puromycine. The expression of DCAF15 was then confirmed by immunoblot analysis.

Amplicon sequencing.

Genomic DNA was extracted using the PureLink(R) Genomic DNA Kit (Thermo), according to the manufacturer's instructions. The genomic DNA was amplified with PrimeSTAR GXL DNA Polymerase (TaKaRa Bio.) with tailed primers

under the following conditions: 98 °C for 2 min; 35 cycles at 98 °C for 10 sec, 55 °C for 15 sec, and 68 °C for 30 sec; and 68 °C for 5 min. A second PCR was then performed for indexing and adaptor addition for the Illumina platform. Here, 2 μL of PCR products were treated with 5 μL of ExoSAP-IT PCR Product Cleanup (USB/Affymetrix), diluted to 1:10, and used as a template. This PCR was performed using NEBNext(R) High-Fidelity 2X PCR Master Mix (New England Biolabs.) under the following conditions: 95 °C for 1 min; 30 cycles at 95 °C for 30 sec, 65 °C for 30 sec, and 72 °C for 3 min; and 72 °C for 5 min. The pooled samples were run on a 2% E-Gel(R) EX Agarose Gel (Thermo) and the correct fragments were gel extracted with the NucleoSpin(R) Gel and PCR Cleanup Kit (MACHEREY-NAGEL GmbH). Purified libraries were quantified with the QuantiFluor dsDNA System (Promega) and run on an Illumina MiSeq (Illumina Inc.).

The MiSeq sequencing run generated Illumina FASTQ files. These files were processed using in-house tools to convert the file format. Data analysis such as sequence filtering, counting reads, and visualization were performed using the TIBCO Spotfire software. The primers used in the amplicon sequencing and indexing are summarized in Supplementary Table 5, 6.

Exome sequencing.

Genomic DNA of parental HCT116 and resistant clonal HCT116 cells were extracted and enriched using the DNeasy Blood & Tissue Kit (Qiagen) and SureSelect Human All Exon V5 (Agilent), according to the manufacturer's protocol. Whole exome sequencing was performed using a HiSeq 2000 (Illumina) with 100 base pairs on each end. The read numbers for the parental HCT116 cell line and resistant clone were 78.4 million and 94.1 million, respectively.

The reads were aligned to the reference genome sequence (GRCh37) using the Burrows-Wheeler Aligner (BWA)[45]. The Genome Analysis Toolkit (GATK) was used for base quality score recalibration, indel realignment, and duplicate removal[46]. To extract drug-resistance-associated mutations, three filters were applied to all locations on the target genome regions with mpileup base frequencies of A, T, G, and C. The first filter was a chi-squared test, which can be used to distinguish differences in base frequencies between sulfonamide-resistant and parental HCT116 cells; the cutoff value for this was set at 0.001. The second filter was a depth filter, whereby the depth of sequence coverage needed to be five or more for both samples. The final filter was a non-synonymous single nucleotide polymorphism filter, which focused on the functional changes caused by the mutations.

Sanger sequencing.

The *CAPERα* fragment was amplified from genomic DNA using PCR primers flanking the R87* and G268V mutations. The PCR products were treated with Exo-SAP-IT (USB/Affymetrix) and sequenced directly with PCR primers. Cycle sequencing was performed using a BigDye Terminator kit, version 3.1 (Applied Biosystems). The products of the sequencing reactions were purified using a Performa DTR Ultra 96-Well Plate Kit (Edge BioSystems) and sequenced in a 16-capillary ABI PRISM 3130xl Genetic Analyzer (Applied Biosystems).

Transcriptional comparison using DNA microarray.

HCT116 cells were seeded in a six-well plate at a density of 1.0×10^5 cells per well with or without the siRNA reverse transfection of the siGENOME SMARTpool of RBM39 (Dharmacon, M-011965) and non-targeting siRNA pool #2 (D-001206-14). Following incubation overnight, DMSO or E7820 were added to the siRNA-free HCT116 plate (final 1 μM of E7820) and incubated for 24 hours. Cells were then harvested using 350 μL of Buffer RLT (Qiagen) containing 1% 2-mercaptethanol (Nakalai tesque) either 48 hours after treatment with the siRNA or 24 hours after

treatment with the compounds, and stored at −80 °C until the next step. All sample groups were prepared with three biological replicates.

Total RNA was prepared using RNeasy mini spin columns (Qiagen), according to the manufacturer's protocol. The yield and quality of each isolated total RNA sample was determined using a NanoDrop 1000 spectrophotometer (Thermo Fisher Scientific) and an RNA Nano LabChip(R) kit analyzed on a 2100 Bioanalyzer (Agilent Technologies). NanoDrop spectrophotometers measure the absorbency at wavelengths of 280 nm and 260 nm, the ratios of which (i.e., A260:A280) are then used to assess sample purity; an A260:A280 ratio of approximately 2.0 is considered pure for RNA samples. By contrast, the 2100 Bioanalyzer calculates an RNA Integrity Number (RIN) based on the pattern of total RNA electrophoresed, which can be used as a metric for RNA degradation (Schroeder et al., 2006); a RIN of 9.7–10.0 is considered pure for total RNA from hiPSC-derived cardiomyocytes.

Total RNA (200 ng) was converted to cyanine-3 (Cy3)-labeled complementary RNA (cRNA) using a Low Input Quick Amp Labeling Kit, One-Color (Agilent Technologies), according to the manufacturer's instructions for single-color 8×60K gene expression arrays. Cy3-labeled cRNAs were purified using an RNeasy Mini purification kit (Qiagen) and hybridized to the SurePrint G3 Human Gene Expression

8×60K Microarray (Agilent Technologies) at 65 °C for 17 hours with a Gene Expression Hybridization Kit (Agilent Technologies), according to the manufacturer's instructions. The arrays were washed with a Gene Expression Wash Pack (Agilent Technologies) and scanned on a DNA Microarray Scanner (Agilent Technologies), according to the manufacturer's instructions. The scanned images were then quantified using Feature Extraction software (version 11.5.1.1, Agilent Technologies), and the resulting files were imported and analyzed with GeneSpring (version 12.5, Agilent Technologies). The raw data were normalized using a quantile method. The differences between treatments were assessed using Welch's t-test, followed by an adjustment for multiple comparisons using the FDR approach (Benjamini-Hochberg procedure). A gene was considered to be differentially expressed when its absolute fold change relative to the control value was ≥ 1.5 with an FDR P-value of ≤ 0.05.

Computational amino acid substitution of CAPERα.

^{268}Glycine in the CAPERα NMR structure PDB:2JRS was mutated to Valine and the side chain of the mutated Valine was energy minimized using CHARMm force field. Modeling and minimization was carried out using Discovery Studio 3.5 (Dassault Systemes, www.3ds.com).

Cell viability assay.

Cells were plated in a 96-well microtiter plates with or without siRNA reverse transfection and incubated overnight. Serial dilutions of compounds were then added to each well. After 3 days, 10 μL of WST-8 reagent (Dojindo) was added to each well. The absorbency at 450 nm (A450) was monitored and compared with a reference measurement at A660 using an EnVision 2103 Multilabel Reader (PerkinElmer), RAINBOW microplate reader (SLT Lab Instruments), or Sunrise microplate reader (TECAN).

Chemistry.

General chemistry procedures;

^{1}H NMR spectra and ^{13}C NMR spectra were recorded on a Varian Mercury 400 spectrometer (operating at 400 MHz) and a Bruker Avance 600 (operating at 150 MHz), respectively. Chemical shifts were calculated in ppm (δ) from the residual CH_3OH signal at δH = 3.31 ppm and δC = 49.0 ppm, or the DMSO signal at δH = 2.50 ppm and δC = 39.7 ppm. ^{1}H NMR data were processed using an ACD/Spectrus Processor from ACD Laboratories. Ultra performance liquid chromatography (UPLC) analyses were

performed using an ACQUITY UPLC system. Column chromatography was carried out using a Hi-Flash column (40 μm, silica gel and NH-silica gel, Yamazen Corporation). Purification and analysis of ^{3}H-E7820 was carried out using HPLC with Gemini C18 column (phenomenex). All chemicals and solvents were purchased from commercial suppliers.

Synthesis of chloroquinoxaline sulfonamide (CQS);

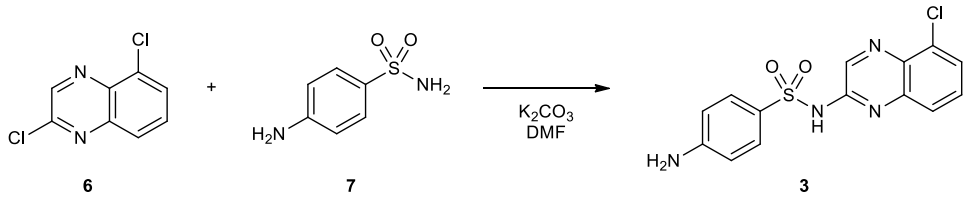

2,5-dichloroquinoxaline[47] (**6**, 500 mg, 2.51 mmol), 4-aminobenzene-1-sulfonamide (**7**, 476 mg, 2.76 mmol), and K_2CO_3 (694 mg, 5.02 mmol) were dissolved in dimethylformamide (DMF) (5 ml). This solution was then stirred at 150 °C for 3 hours, following which the reaction was poured into water (5 mL) and filtered. The filtrate was acidified to pH 4 by adding aqueous HCl, resulting in the precipitation of a yellow solid. The filter cake was dried in vacuo and the residue was purified by column chromatography (petroleum ether / ethyl acetate. 5:1) to give CQS (**3**, 244 mg, 0.730 mmol, 29% yield) as a yellow solid. **^{1}H NMR** (400 MHz, DMSO-d_6): δ ppm = 6.07 (brs, 2H), 6.43–6.70 (m, 2H), 7.55–7.91 (m, 5H), 8.59 (s, 1H), 11.72 (brs,

1H). **^{13}C NMR** (150 MHz, DMSO-d_6): δ ppm = 112.4, 123.7, 126.7, 127.3, 130.4, 130.9, 132.1, 134.7, 139.0, 141.3, 147.0, 153.7. **LC-MS**: *m/z* = 335 [M+H], 333 [M-H].

Preparation of tritium-labeled E7820;

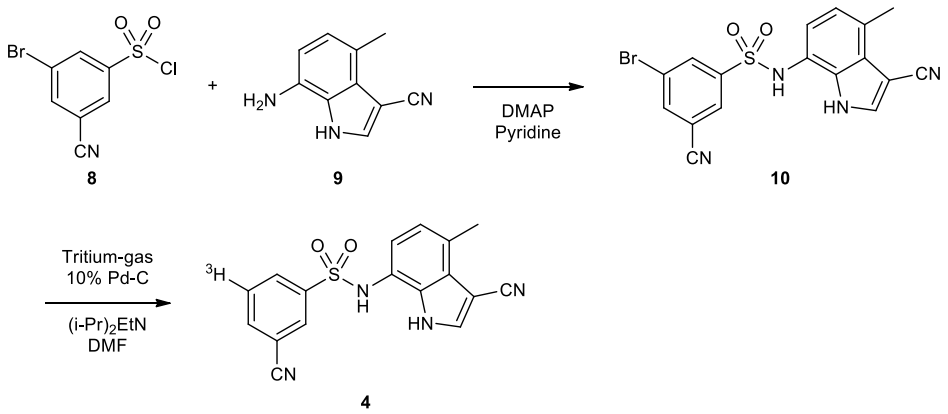

3-Bromo-5-cyano-*N*-(3-cyano-4-methyl-1*H*-indol-7-yl)benzenesulfonamide;

3-Bromo-5-cyanobenzene-1-sulfonylchloride (**8**, 0.30 g, 1.1 mmol), 7-amino-3-cyano-4- methylindole (**9**, 0.17 g, 0.98 mmol)[48], and 4-dimethyaminopyridine (0.28 g, 0.25 mmol) were dissolved in 2 mL of pyridine, and the solution was stirred at room temperature (rt) for 5 hours. The solution was then diluted with ethyl acetate (AcOEt), and washed with 0.1 N HCl followed by brine, dried over $MgSO_4$, and evaporated to provide a slightly colored solid. This was then filtrated and washed with MeOH to provide the product (**10**, 0.30 g, 0.72 mmol, 82% yield). **^{1}H-NMR** (400 MHz, DMSO-*d*6): δ ppm = 12.12 (brs, 1H), 10.21 (brs, 1H), 8.49 (s, 1H), 8.21 (s, 1H), 8.08 (s, 1H), 8.04 (s, 1H), 6.84 (d, *J* = 7.6 Hz, 1H), 6.53 (d, *J* = 7.6 Hz,

1H), 2.60 (s, 3H). **^{13}C NMR** (150 MHz, DMSO-d_6): δ ppm = 17.9, 84.6, 114.5, 116.3, 117.4, 119.4, 120.2, 122.7, 123.0, 126.9, 129.0, 129.7, 131.7, 133.9, 135.7, 139.2, 142.1. **LC-MS**: *m/z* = 415, 417 [M+H].

3-Cyano-*N*-(3-cyano-4-methyl-1*H*-indol-7-yl)-[5-^{3}*H*]-benzenesulfonamide;

3-Bromo-5-cyano-*N*-(3-cyano-4-methyl-1*H*-indol-7-yl)benzenesulfonamide (5 mg, 12 μmol) and 10% Pd-C (10 mg) were added to in the solution of 1 mL of DMF and 10 μL of *N,N*-diisopropylethylamine. The mixture was stirred under tritium gas (111 GBq) for 2 hours. The mixture was then diluted with EtOH and the catalyst was removed by filtration. The crude product was purified by high-performance liquid chromatography (HPLC) (25 × 0.96 cm Ultrasphere ODS column in an H_2O/MeCN/TFA system) using 3-cyano-*N*-(3-cyano-4-methyl-1*H*-indol-7-yl)benzenesulfonamide as a reference. The purified fraction was evaporated to dryness and dissolved in EtOH as a 189 MBq/mL solution. **MS**: *m/z* = 337, 339 [M+H]. **Radiochemical purity**: 99.7% by HPLC. **Specific activity**: 629 GBq/mmol.

Preparation of the biotinyl photoactive E7820 probe;

The validity of using linker substitution in a sulfonamide compound has been described previously[49].

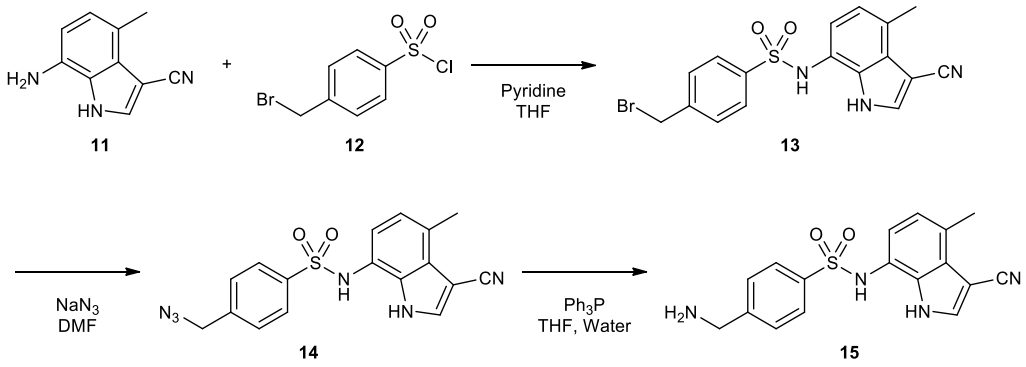

7-amino-4-methyl-1*H*-indole-3-carbonitrile (**11**, 300 mg, 1.76 mmol) was dissolved in 5 ml of tetrahydrofuran (THF) at 0 °C. Pyridine (0.356 ml, 4.40 mmol) was then added to the solution. After 10 min, 4-(bromomethyl)benzene-1-sulfonylchloride (**12**, 712 mg, 2.64 mmol) in 5 ml of THF was added to the reaction mixture and the mixture was stirred at rt overnight. The reaction mixture was then diluted with EtOAc (30 ml) and poured onto a sat. aq. NH_4Cl solution (50 ml). The organic phase was separated from the aqueous solution, washed with brine (50 ml), and dried over $MgSO_4$ and filtered. The organic phase was then evaporated to yield the crude product. Silica gel chromatography eluting with 30–100% EtOAc-heptane provided a mixture of 4-(bromomethyl)-*N*-(3-cyano-4-methyl-1*H*-indol-7-yl)benzene-1-sulfonamide (**13**), which was used in the next step without further purification.

The obtained product (**13**, 712 mg) was dissolved in DMF (14.6 ml). Sodium azide (572 mg, 8.81 mmol) was then added to the solution, which was stirred overnight at rt. The mixture was poured into water and extracted with ethyl acetate/diethyl ether ($EtOAc/Et_2O$, 1:1). The organic phase was separated from the aqueous solution and washed with brine, dried over $MgSO_4$, and concentrated under reduced pressure. The crude product was then purified by silica gel column chromatography (20–60% EtOAc in heptane) to provide

4-(azidomethyl)-*N*-(3-cyano-4-methyl-1*H*-indol-7-yl)benzene-1-sulfonamide (**14**, 89.5 mg, 13.9% yield). **^{1}H NMR** (400 MHz, DMSO-*d*6): δ ppm = 2.56 (s, 3H), 4.56 (s, 2H), 6.53 (d, *J* = 7.6 Hz, 1H), 6.75 (d, *J* = 1 Hz, 7.6 Hz, 1H), 7.50 (d, *J* = 7.2 Hz, 2H), 7.71 (brd, *J* = 7.2 Hz, 2H), 8.16 (s, 1H), 9.95 (brs, 1H), 11.53 (brs, 1H). **^{13}C NMR** (150 MHz, DMSO-d_6): δ ppm = 17.8, 52.9, 84.5, 117.5, 118.8, 120.5, 122.5, 126.7, 127.5, 127.8, 128.9, 131.0, 135.4, 138.8, 141.0. **LC-MS**: *m/z* = 367 [M+H], 389 [M+Na].

4-(Azidomethyl)-*N*-(3-cyano-4-methyl-1*H*-indol-7-yl)benzenesulfonamide (500 mg, 1.365 mmol) was dissolved in THF/water (10:1). Triphenylphosphine (537 mg, 2.047 mmol) was then added to the solution and the reaction mixture was stirred at 60 °C for 8 hours. The mixture was concentrated under reduced pressure and the precipitated white solid was collected by paper filtration. The solid was washed with

CH_2Cl_2 and dried in vacuo to obtain

4-(aminomethyl)-*N*-(3-cyano-4-methyl-1*H*-indol-7-yl)benzenesulfonamide (**15**, 388 mg, 1.140 mmol, 84% yield). **^{1}H NMR** (400 MHz, DMSO-*d*6): δ ppm = 3.17 (s, 2H), 3.84 (s, 3H), 6.64 (s, 2H), 7.42 (d, *J* = 8.06 Hz, 3H), 7.68 (d, *J* = 8.25 Hz, 3H), 8.00 (s, 1H). **^{13}C NMR** (150 MHz, DMSO-d_6): δ ppm = 17.7, 44.0, 83.9, 115.4, 118.1, 122.7, 123.0, 126.1, 126.6, 126.8, 127.9, 130.7, 134.2, 141.3, 144.0. **LC-MS**: *m/z* = 341 [M+H].

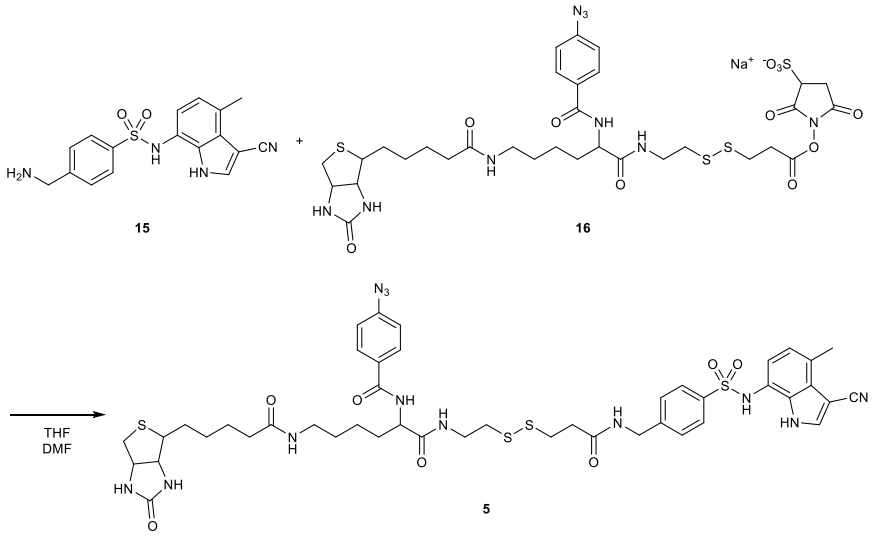

4-(Aminomethyl)-*N*-(3-cyano-4-methyl-1*H*-indol-7-yl)benzenesulfonamide (**15**, 4.26 mg, 0.013 mmol), triethylamine (4.75µl, 0.034mmol) and sodium 1-({3-[(2-{[2-(4-azidobenzamido)-6-{[5-(2-oxohexahydro-1*H*-thieno[3,4-*d*]imidazol-4-yl)pentanoyl]amino}hexanoyl]amino}ethyl)disulfanyl]propanoyl}oxy)-2,5-dioxopyrrolidine-3-sulfonate (**16**, 10 mg, 0.011 mmol) (Thermo Fisher Scientific, #33033) were

dissolved in DMF (1 ml) and stirred overnight at rt. The reaction mixture was then concentrated under reduced pressure and the obtained residue was purified by silica gel flash chromatography (10–20% methanol in ethylacetate) to provide the target biotinyl photoactive chemical probe,

4-azido-*N*-[1-{4-[(3-cyano-4-methyl-1*H*-indol-7-yl)sulfamoyl]phenyl}-3,11,18-trioxo-2 2-(2-oxohexahydro-1*H*-thieno[3,4-*d*]imidazol-4-yl)-6,7-dithia-2,10,17-triazadocosan-12 -yl]benzamide (**5**, 10.4 mg, 10.37 μmol, 91% yield). **^{1}H NMR** (400 MHz, METHANOL-*d*4): δ ppm = 1.36–1.92 (m, 12H), 2.15 (t, *J* = 7.06 Hz, 2H), 2.62 (s, 3H), 2.62–2.3 (m, 4H), 2.83 (t, *J* = 6.78 Hz, 2H), 2.97 (t, *J* = 6.78 Hz, 2H), 3.12–3.20 (m, 2H), 3.42–3.59 (m, 3H), 4.26 (dt, *J* = 7.70, 3.85 Hz, 1H), 4.40 (s, 2H), 4.42–4.51 (m, 2H), 4.62 (brs, 1H), 6.47 (d, *J* = 7.70 Hz, 1H), 6.71 (d, *J* = 7.51 Hz, 1H), 7.09 (d, *J* = 8.25 Hz, 2H), 7.37 (d, *J* = 8.25 Hz, 2H), 7.59 (d, *J* = 8.25 Hz, 2H), 7.82–7.94 (m, 3H). **^{13}C NMR** (150 MHz, DMSO-d_6): δ ppm = 18.3, 24.5, 26.9, 29.4, 29.7, 30.1, 32.7, 35.3, 36.5, 36.8, 38.5, 39.6, 40.0, 41.0, 43.6, 55.6, 57.0, 62.3, 63.4, 86.1, 118.6, 119.9, 121.5, 121.8, 123.8, 128.3, 128.7, 128.9, 130.1, 130.5, 131.6, 133.2, 135.5, 139.2, 145.1, 145.6, 166.1, 169.2, 173.8, 174.7, 176.1. **LC-MS**: *m/z* = 1003 [M+H].

Data availability.

Proteome, exome sequencing, and DNA microarray data have been deposited in the jPOST (accession code: JPST000232), NCBI (accession code: SRP097451), and GEO (accession code: GSE93829), respectively.

Figures

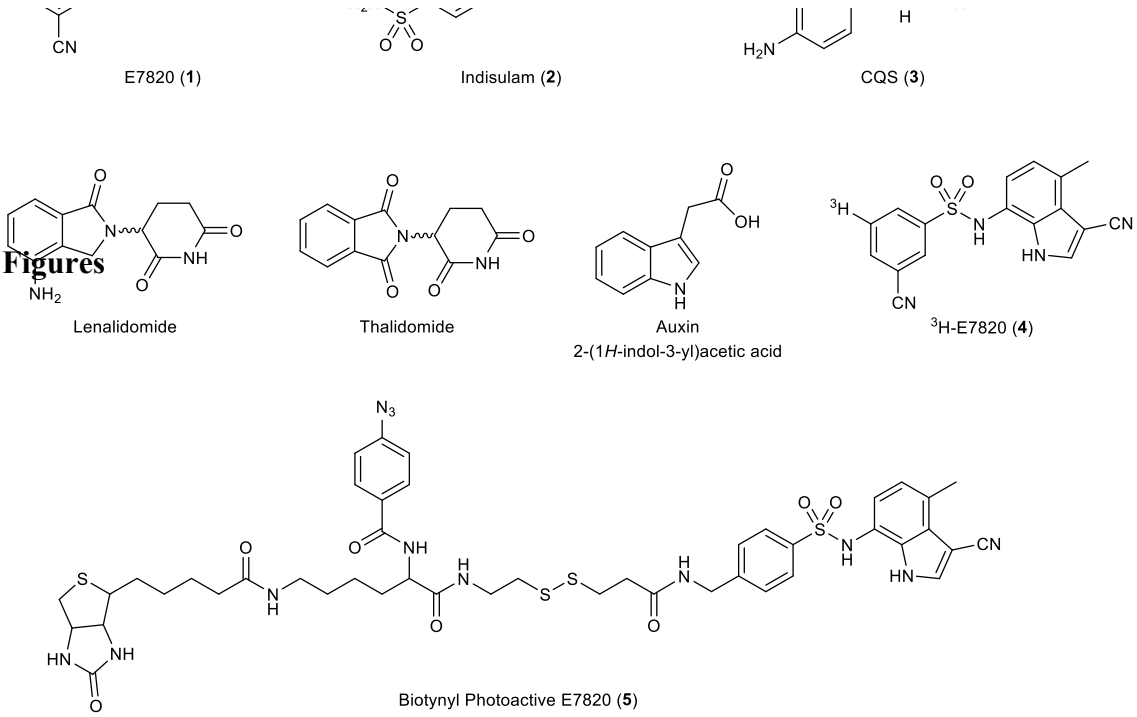

Figure II-1. Chemical structures of the anticancer sulfonamides E7820 (1), indisulam (2), and CQS (3), immunomodulatory drugs (IMiDs) lenalidomide and thalidomide, auxin, ^{3}H-E7820 (4), and the biotynyl photoactive E7820 probe (5).

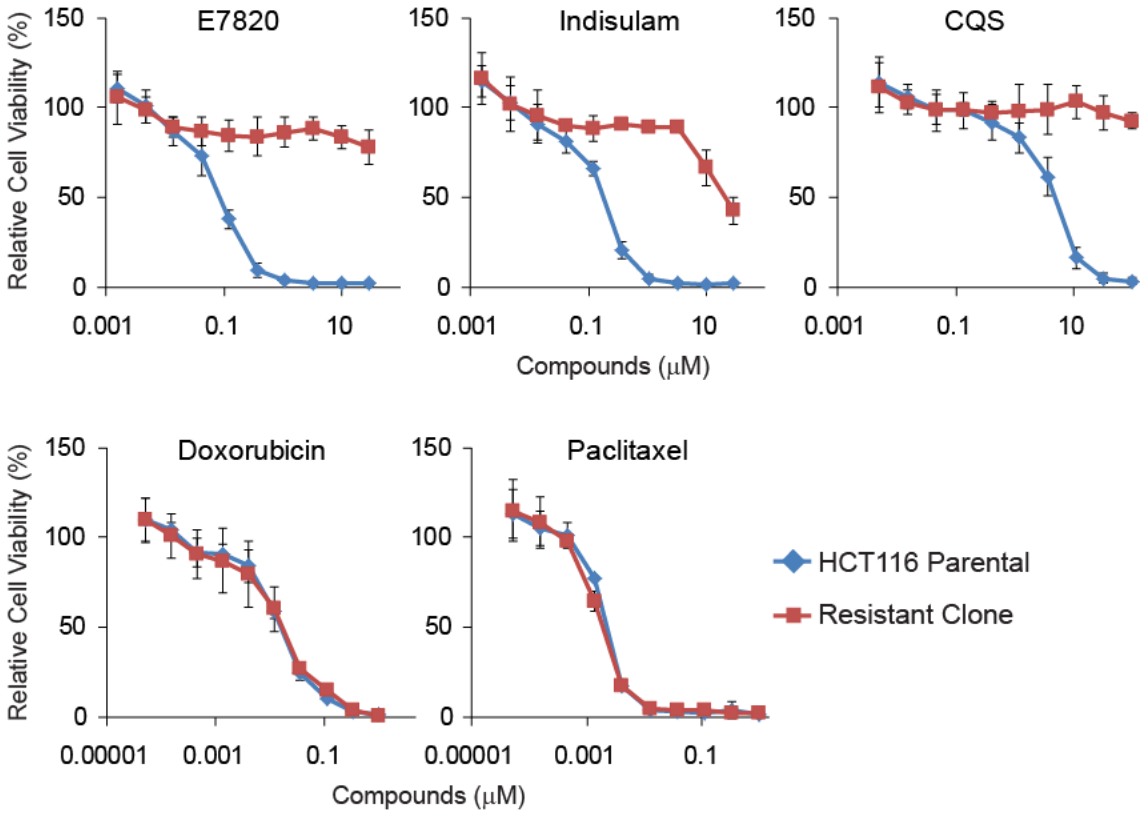

Figure II-2. Cell viability assay results for the parental HCT116 human colorectal cancer cell line and a spontaneously occurring indisulam-resistant subclonal cell line. Cells were treated with E7820, indisulam, and chloroquinoxaline sulfonamide (CQS), and the cytotoxic agents doxorubicin and paclitaxel. Data are presented as the mean of three independent experiments ± SD.

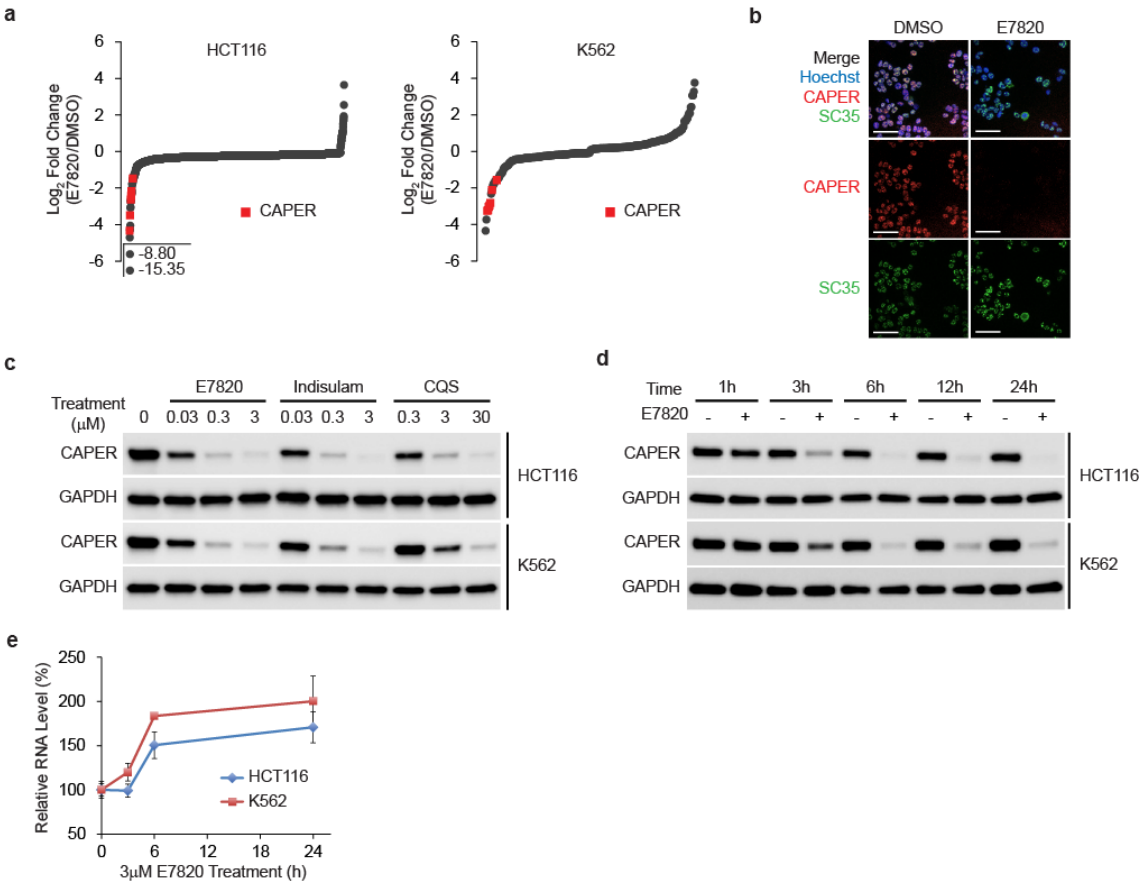

Figure II-3. Down-regulation of CAPERα by E7820, indisulam, and CQS. (**a**) Proteome-wide analysis of HCT116 and K562 cells treated with 3 μM E7820 or DMSO for 6 hours. Each point represents the $\log_2$ ratio of mean tryptic peptide ion peaks in E7820- versus DMSO-treated cells (n = 3, $P < 0.05$). (**b**) *In vitro* cell staining of HCT116 cells treated with 3 μM E7820 or DMSO for 22 hours. Scale bars, 50 μm. (**c**) Immunoblot analysis of HCT116 and K562 cells treated with the indicated concentrations of E7820, indisulam, CQS, or DMSO for 24 hours. (**d**) Time course of CAPERα protein levels and (**E**) mRNA levels in HCT116 and K562 cells treated with 3 μM E7820 or DMSO. Immunoblot results are representative of two independent experiments. qPCR data are presented as the mean ± SD (*n* = 3).

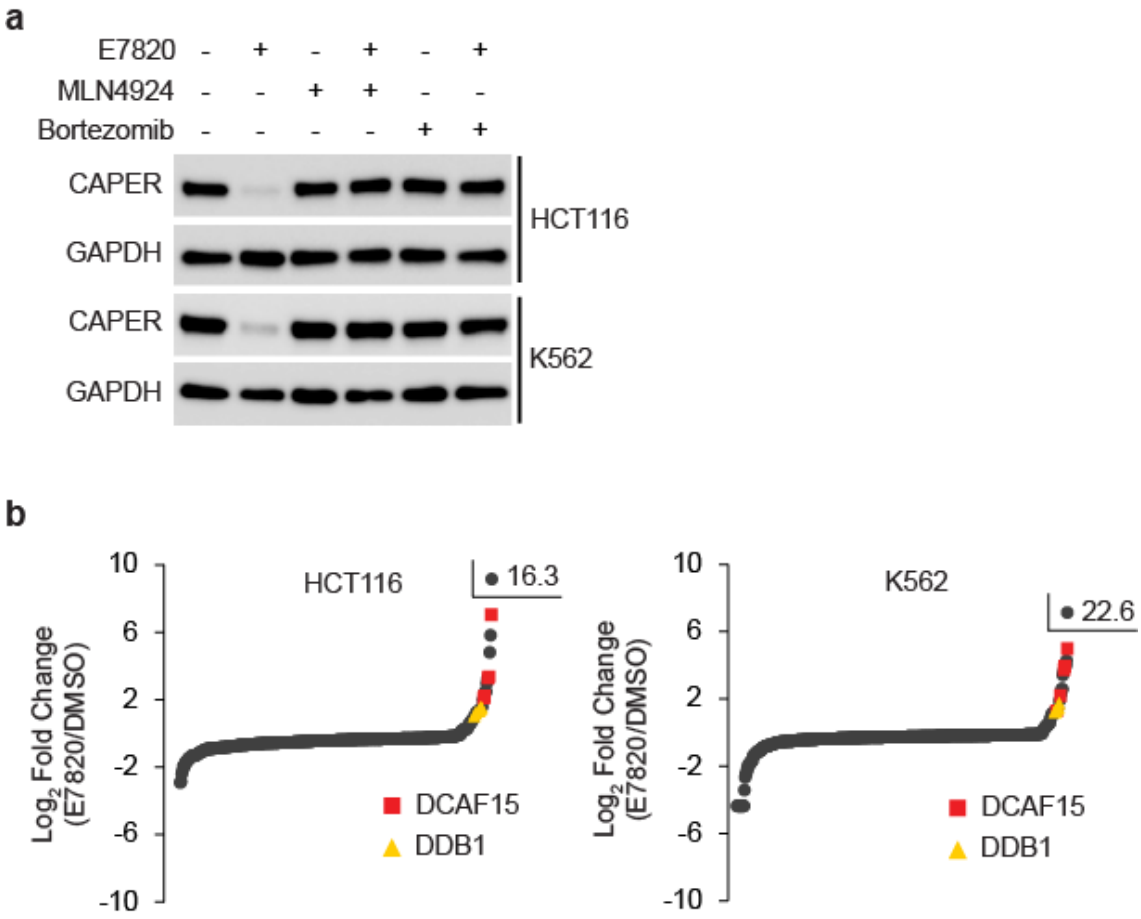

Figure II-4. E7820, indisulam, and CQS promote CRL4^{DCAF15} mediated CAPERα degradation. (**a**) Chemical rescue of CAPERα degradation in HCT116 and K562 cells treated with 3 μM E7820 or DMSO for 6 hours. Cells were pretreated with MLN4924 (1 μM) or bortezomib (0.2 μM) before the addition of E7820. (**b**) CAPERα interaction analysis of HCT116 and K562 cells treated with E7820 (1 μM) or DMSO for 6 hours. Each point represents the $\log_2$ ratio of the mean tryptic peptide ion peak following CAPERα co-immunoprecipitation in E7820- versus DMSO-treated cells ($n = 3$, $P < 0.05$).

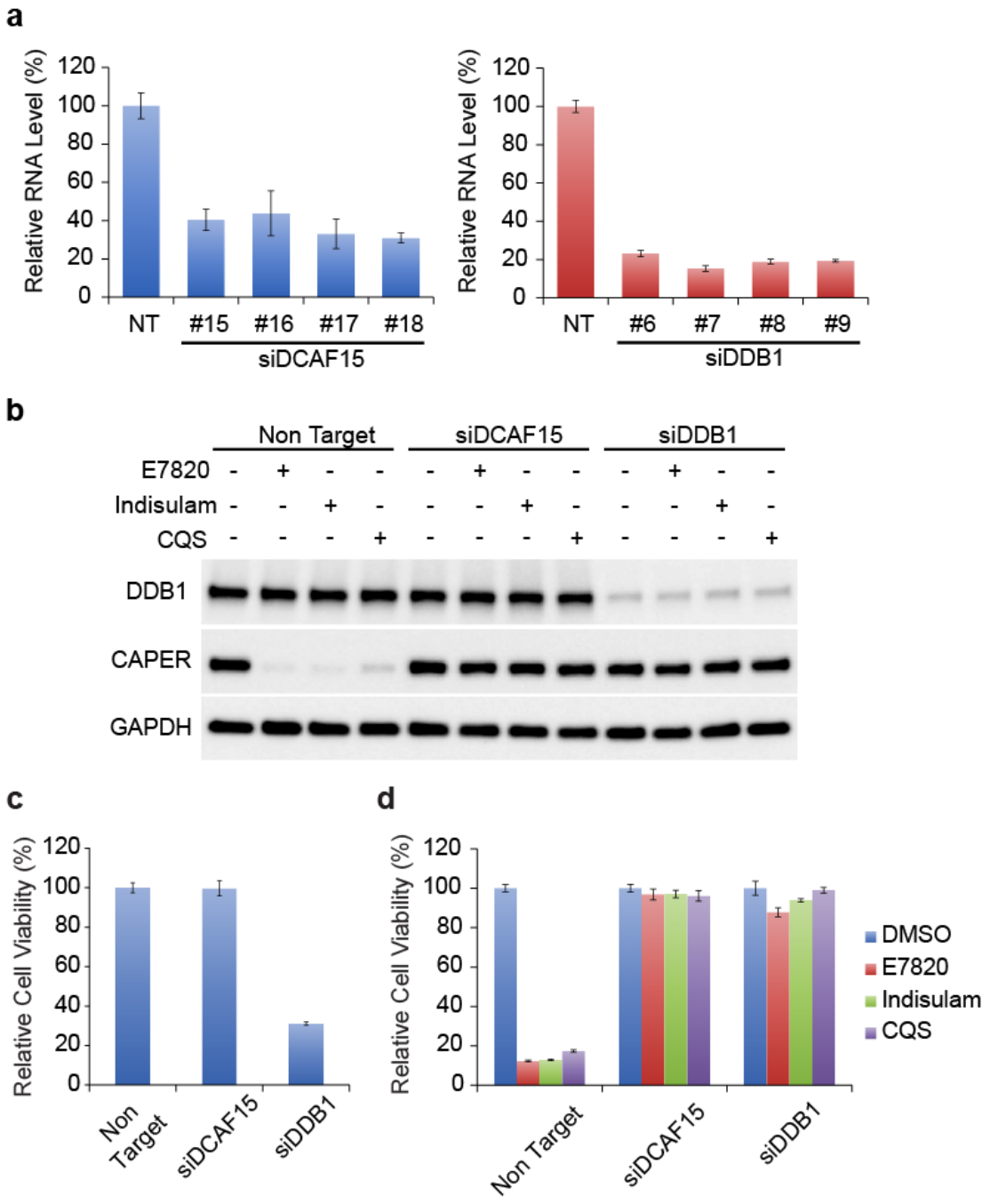

Figure II-5. siRNA-mediated knockdown of DCAF15 and DDB1 in HCT116 cells.

(**a**) Reductions in mRNA expression by siDCAF15 and siDDB1 were assessed using quantitative polymerase chain reaction (qPCR). Cells were transfected with siRNA and incubated for 2 days. Data are presented as mean ± SD (n = 3). (**b**) Effect of sulfonamides on CAPERα in siRNA-transfected cells. Cells were transfected with

siRNA and incubated for 2 days, and then treated with E7820 (3 μM), indisulam (3 μM), CQS (30 μM), or DMSO for 6 hours. (**c**) Viability of HCT116 cells with siRNA-mediated knockdown of DCAF15 or DDB1. Cell viabilities were normalized with the viability of non-target siRNA treated cell. Data are presented as mean ± SD (n = 3). (**d**) Cell viability of HCT116 cells with siRNA mediated gene knockdown and sulfonamide treatment. Cell viabilities were normalized with the viabilities of DMSO control cells in each siRNA treatment group. Data are presented as mean ± SD (n = 3). Cells were transfected with siRNA and incubated for 1 day, and then treated with E7820 (3 μM), indisulam (3 μM), CQS (30 μM), or DMSO for 72 hours.

a

Wild Type	CGCTCACCATCCTCCGGCTCCGTCCCCTCTCCGGACTCCAGC ACATAGTACAGCTTGGTGTAGTTGACATAGCCAGGCTCGGA GGCAGGTGCCTCCGAGG
Insertion-A	CGCTCACCATCCTCCGGCTCCGTCCCCTCTCCGGACTCCAGC ACATAGTACAAGCTTGGTGTAGTTGACATAGCCAGGCTCGGA GGCAGGTGCCTCCGAG
Insertion-T	CGCTCACCATCCTCCGGCTCCGTCCCCTCTCCGGACTCCAGC ACATAGTACTAGCTTGGTGTAGTTGACATAGCCAGGCTCGGA GGCAGGTGCCTCCGAG

b

Gene Sequencing of DCAF15		HCT116 Parent	HCT116 *DCAF15-/-*
Total Lead Number		55679	70183
Relative Lead Number (%)	Wild Type	100	0
	Insertion-A	0	49.86
	Insertion-T	0	45.47
	Others	0	4.67

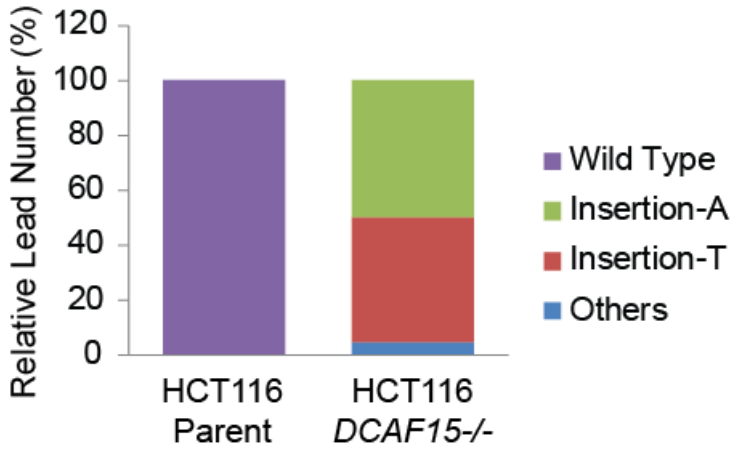

Figure II-6. CRISPR/Cas9-based DCAF15 knockout in HCT116 cells. (**a**) Gene sequences of the wild type and the line exhibiting a single nucleotide insertion of DCAF15 by CRISPR/Cas9. (**b**) DCAF15 allele ratio in parental HCT116 and its

DCAF15 knockout clonal cells analyzed by amplicon sequencing. Short reads (< 100 bp long) and minor reads (< 1% frequency) were excluded from the analysis.

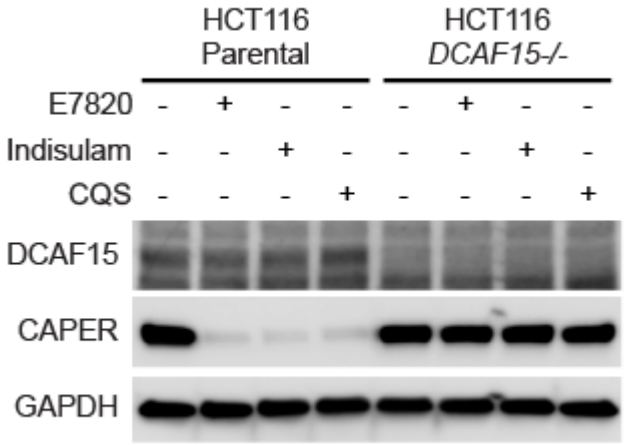

Figure II-7. Immunoblot analysis of parental and DCAF15 knockout clones of HCT116 cells. Cells were treated with E7820 (3 μM), indisulam (3 μM), CQS (30 μM), or DMSO for 6 hours.

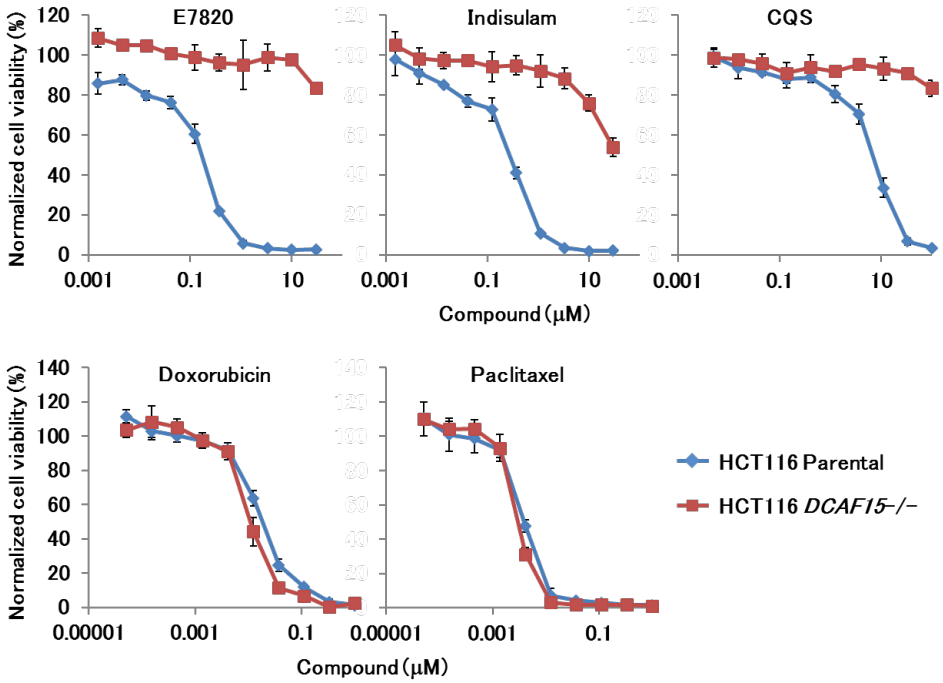

Figure II-8. Growth inhibitory curves of anticancer sulfonamides and cytotoxic agents in parental and *DCAF15*-/- HCT116 cells. Data are presented as the mean ± SD (n = 3).

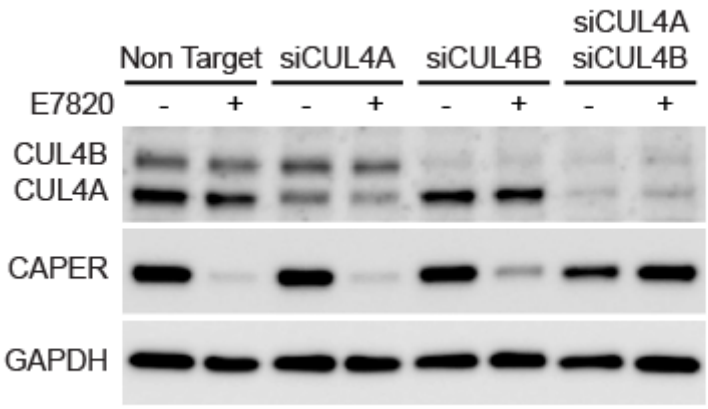

Figure II-9. siRNA-mediated knockdown of CUL4A and CUL4B in HCT116 cells.

Effect of sulfonamides on CAPERα in siRNA-transfected cells. Cells were transfected with siRNA and incubated for 2 days, and then treated with E7820 (3 μM), indisulam (3 μM), CQS (30 μM), or DMSO for 6 hours.

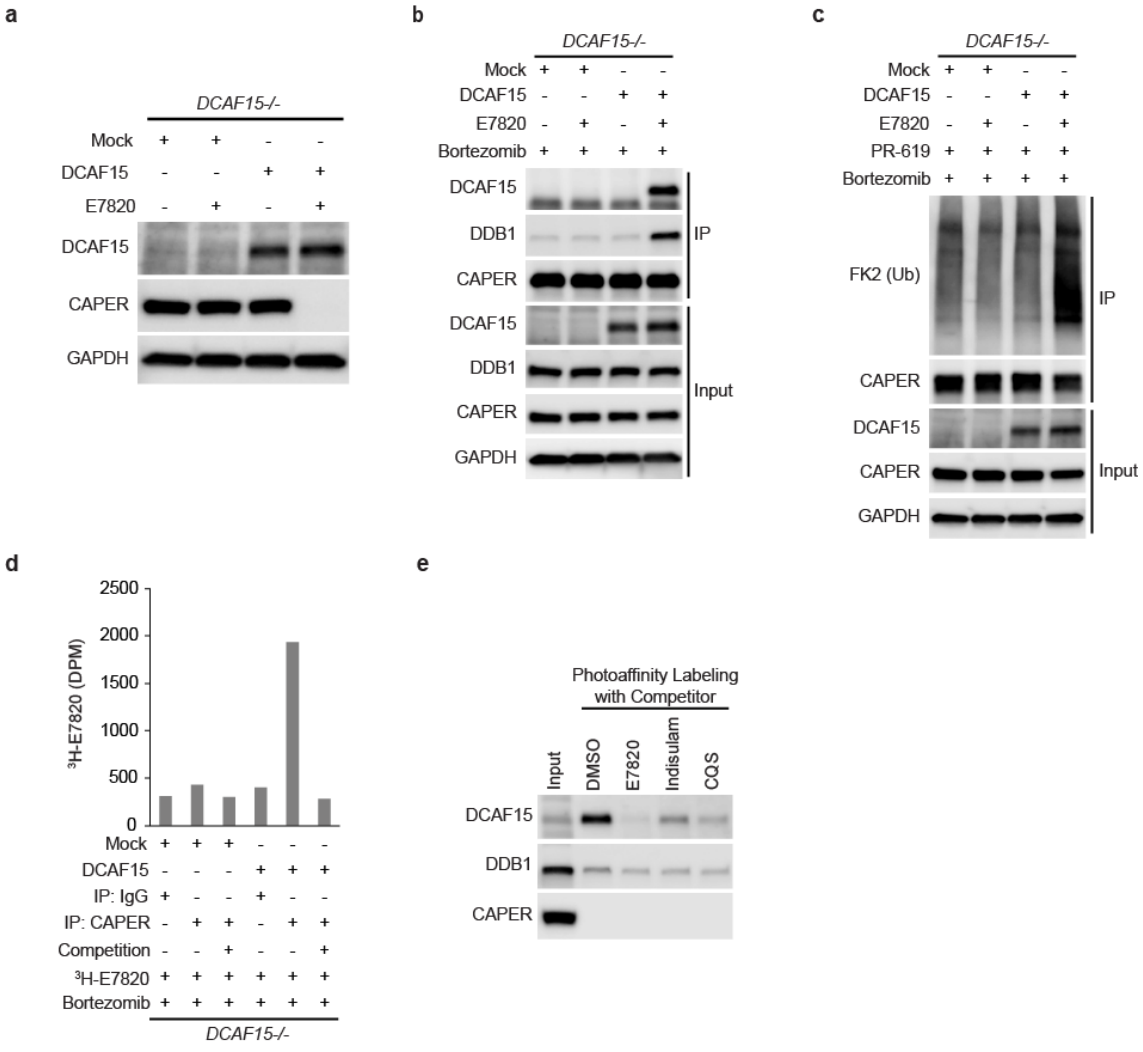

Figure II-10. DCAF15 is the primary target of E7820, indisulam, and CQS in the ubiquitination of CAPERα. (**a**) Effect of sulfonamides on CAPERα in DCAF15 and mock-vector-transfected *DCAF15*-/- HCT116 cells treated with 3 μM E7820 or DMSO for 6 hours. (**b**) Immunoprecipitation and immunoblot analysis of the CAPERα binding protein. Cells were pretreated with bortezomib (0.5 μM) before treatment with E7820 (3 μM) or DMSO for 3 hours. IP, immunoprecipitation with anti-CAPERα antibody. (**c**) Cell-based ubiquitination analysis of endogenous CAPERα. Cells were pretreated with bortezomib (0.5 μM) before treatment with E7820 (3 μM) or DMSO, and the de-ubiquitination inhibitor PR-619 (30 μM), as indicated, for 3 hours. IP,

immunoprecipitation with anti-CAPERα antibody. (**d**) ^{3}H-E7820 pulldown by CAPERα immunoprecipitation. Cells were pretreated with bortezomib (0.5 μM), and then treated with ^{3}H-E7820 (1 μM) for 3 hours with or without cold E7820 competition (20 μM). Data are the mean of two cycle analyses. (**e**) Photoaffinity labeling of target protein with the biotinylated photoactive E7820 probe. The DCAF15-vector-transfected *DCAF15*-/- HCT116 cell lysate with or without competition of the sulfonamide derivatives (30 μM) that had been incubated with the E7820 probe for 30 min followed by UV irradiation. Labeled proteins were enriched using streptavidin beads followed by immunoblot analysis.

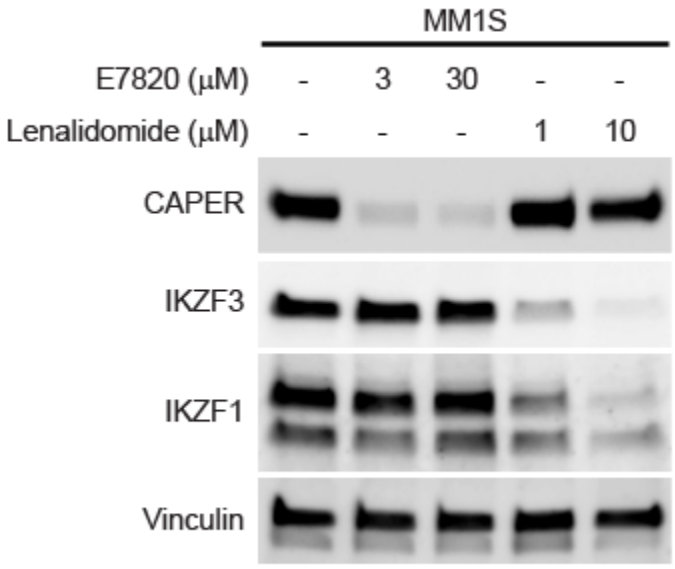

Figure II-11. Degradation of CAPERα, IKZF1, and IKZF3 in MM.1S cells.

Immunoblot analyses of MM.1S cells treated with DMSO, E7820 (3 or 30 μM), or lenalidomide (1 or 10 μM) for 12 hours.

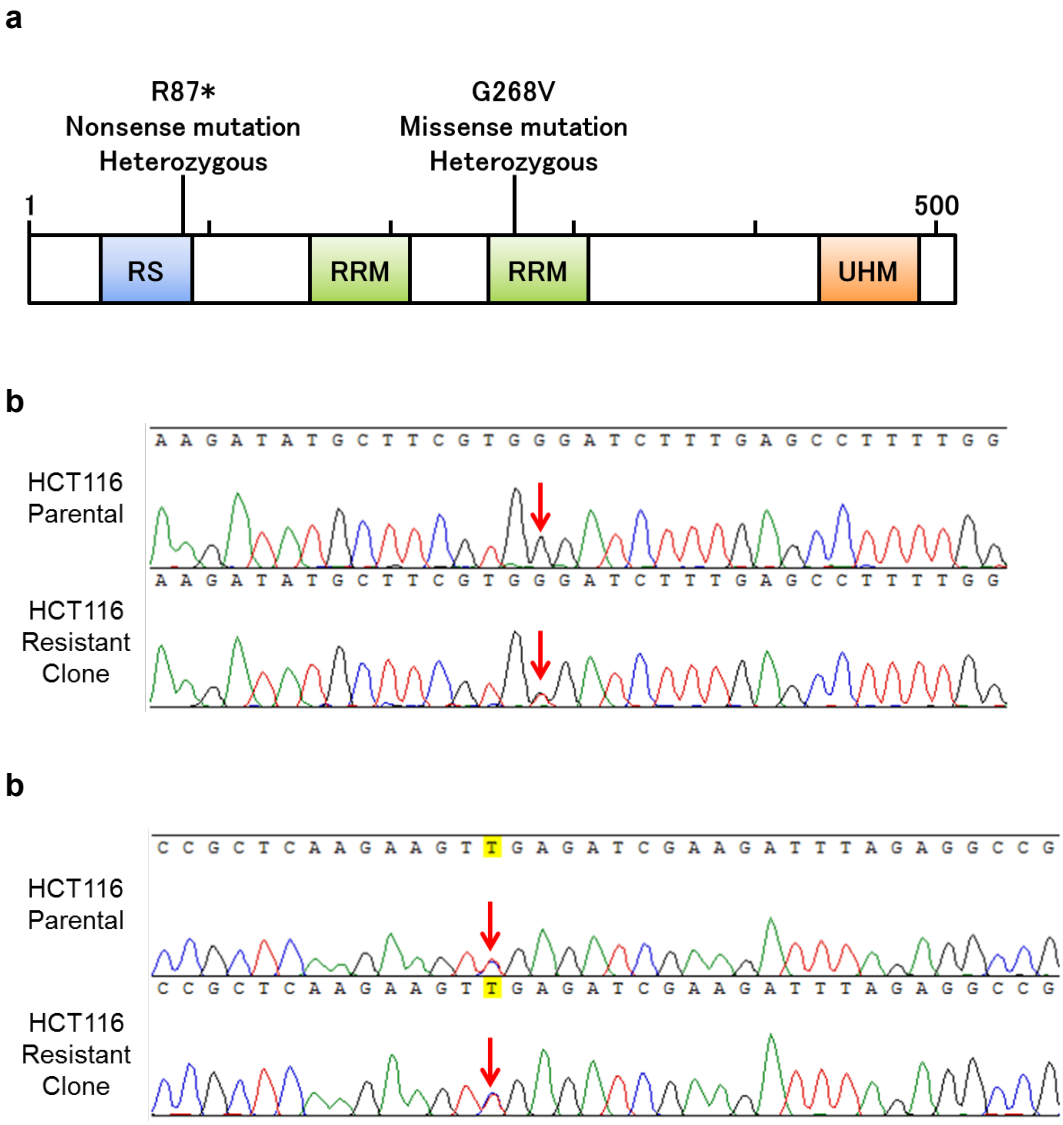

Figure II-12. Discovery of the *CAPERα* mutations in parental HCT116 and spontaneously generated sulfonamide-resistant clonal cells. (a) Mapping of the *CAPERα* mutation in sulfonamide-resistant HCT116 cells. (**b**) Sanger sequencing of G268V missense mutation and (**c**) R87-nonsense mutation in the parental HCT116 and sulfonamide-resistant clonal cells.

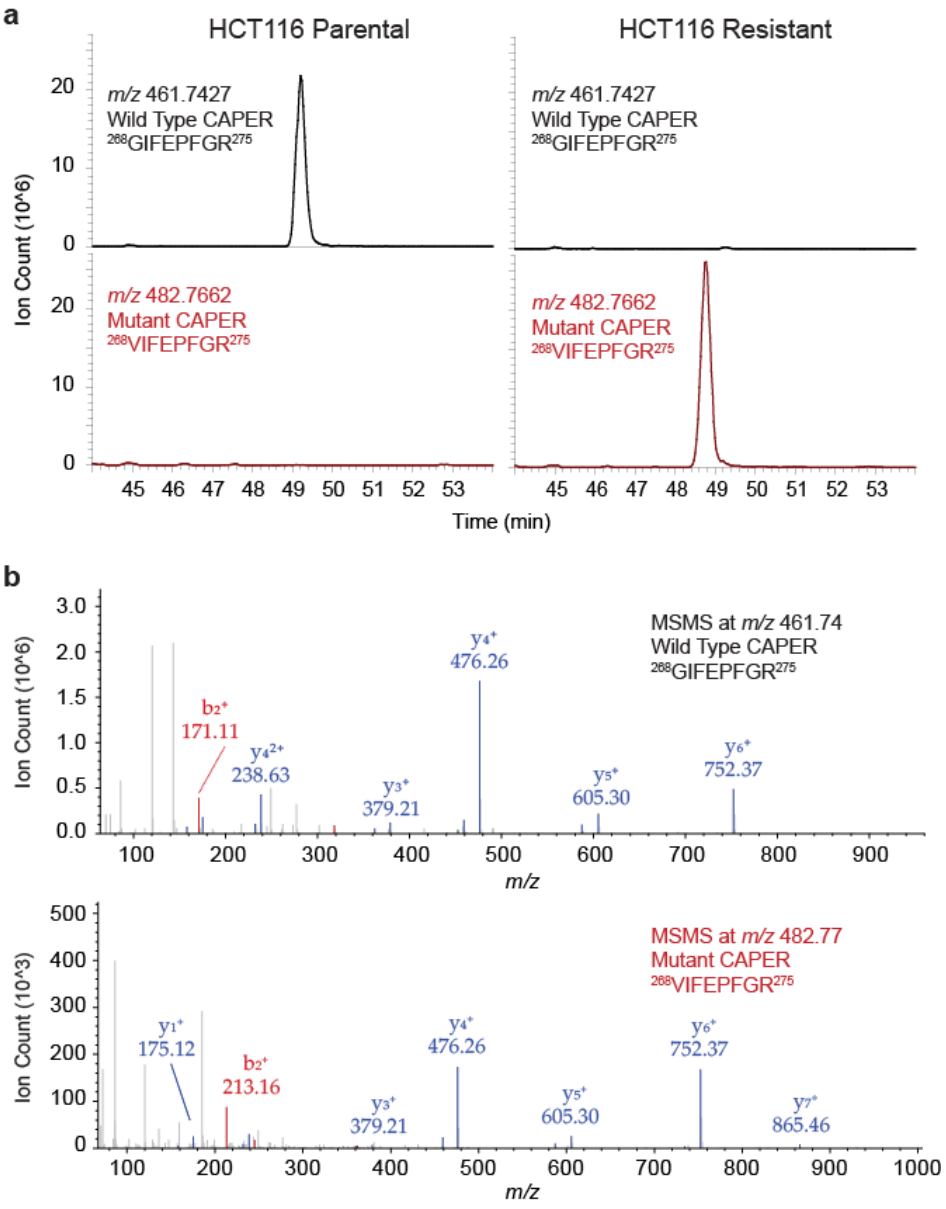

Figure II-13. Immunoprecipitation-LC-MS/MS analysis of CAPERα in the parental HCT116 cells and spontaneously appearing sulfonamide-resistant clonal cells. (**a**) Mass chromatograms of the wild type and mutant peptides from trypsinized CAPERα. Results are representative of two independent experiments. (**b**) MS/MS spectra of the wild type and mutant peptides from trypsinized CAPERα.

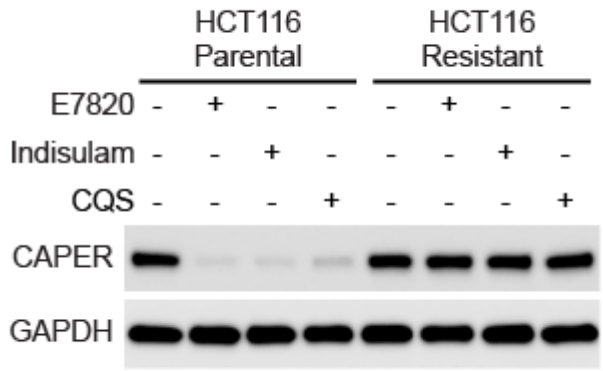

Figure II-14. Immunoblot analysis of parental and sulfonamide-resistant HCT116 cells. Cells were treated with E7820 (3 μM), indisulam (3 μM), CQS (30 μM), or DMSO for 6 hours. Results are representative of two independent experiments.

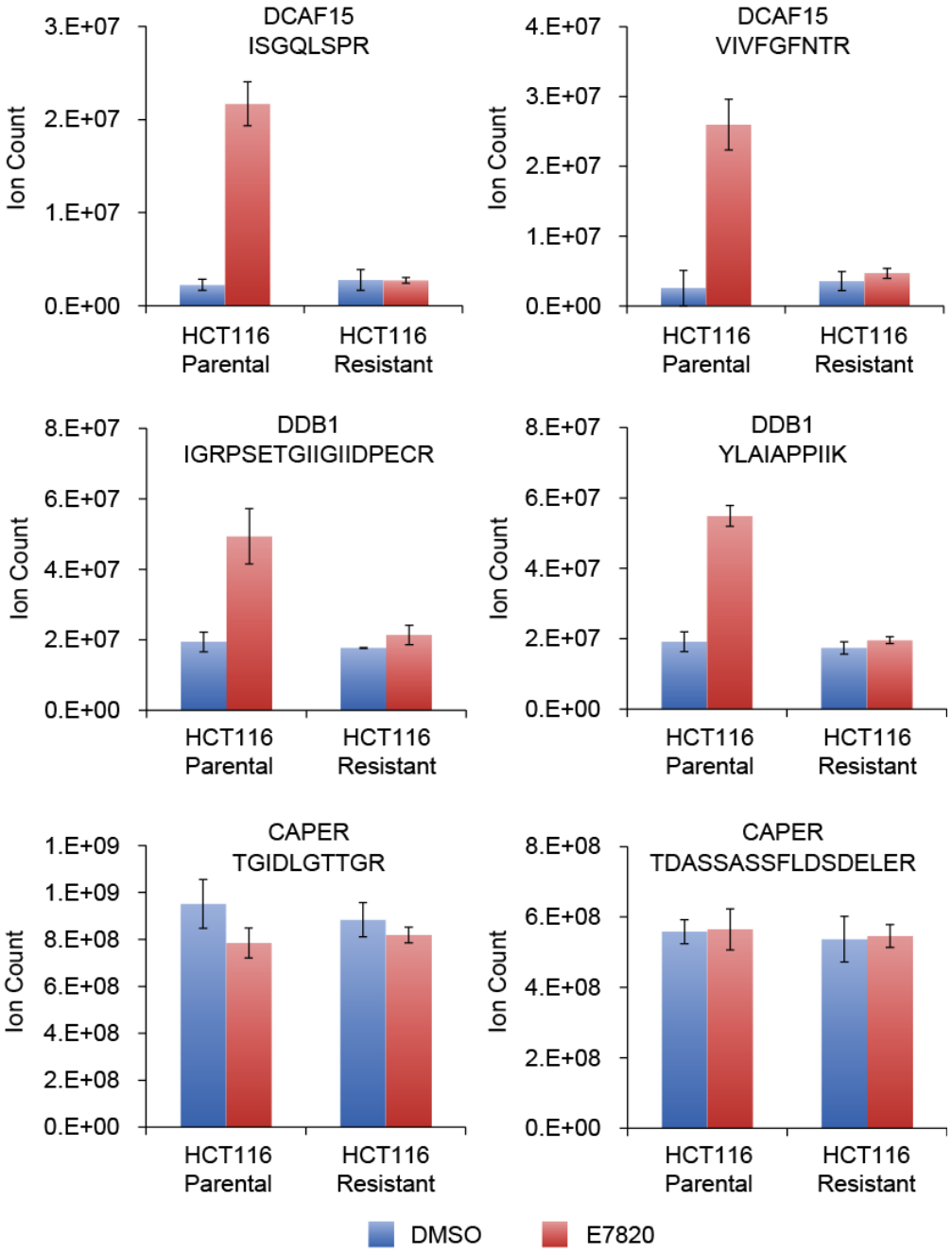

Figure II-15. Co-immunoprecipitation/liquid chromatography-tandem mass spectrometry (LC-MS/MS) analysis of CAPERα. Parental HCT116 or sulfonamide-resistant clonal cells were treated with either E7820 or DMSO for 3 hours. Data are presented as the mean of the LC-MS/MS peak areas ± SD (n = 3).

a

Wild Type	GGCTTTATGTGGGCTCATTACACTTCAACATAAC TGAAGATATGCTTCGT**GGG**ATCTTTGAGCCTTTT GGAAGAGTAAGTCCAGGTTCTTCAATGAATCTT CAGTAGGTTGTTGATCTGAGTATAACTACAT
G268V-CRISPR	GGCTTTATGTGGGCTCATTACACTTCAACATAAC TGAAGATATGCTTCGT**GTT**ATCTTTGAGCCTTTT GGAAGAGTAAGTCCAGGTTCTTCAATGAATCTT CAGTAGGTTGTTGATCTGAGTATAACTACAT

b

CAPER/RBM39 Sequencing		Bulk	E7820 selected	G268V clone
Total Lead Number		476225	392541	158846
Relative Lead Number (%)	Wild Type	97.4	15.4	62.7
	G268V	1.2	66.5	37.3
	Others	1.5	18.1	0.0

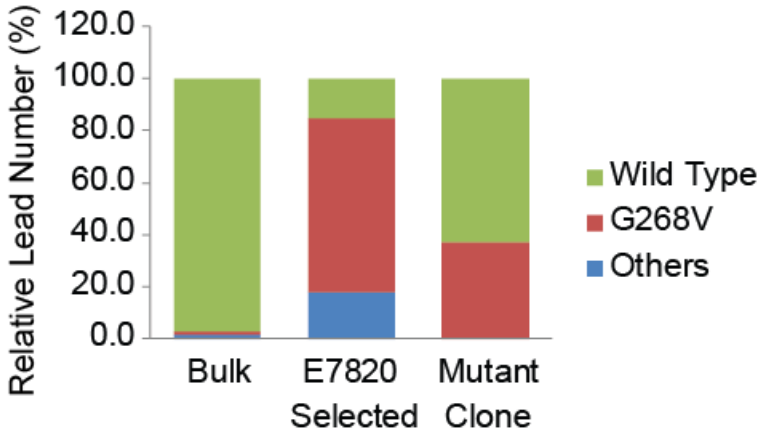

Figure II-16. Biological confirmation of the mutation-based resistance of CAPERα.

(**a**) Gene sequences of the wild type and edited G268V CAPERα. (**b**) CAPERα amplicon sequencing of bulk K562 cells with transfection of the CRISPR/Cas9 system, following enrichment by E7820 treatment, and a clonal cell obtained from

E7820-treated cells. Short reads (< 100 bp long) and minor reads (< 1% frequency) were excluded from the analysis.

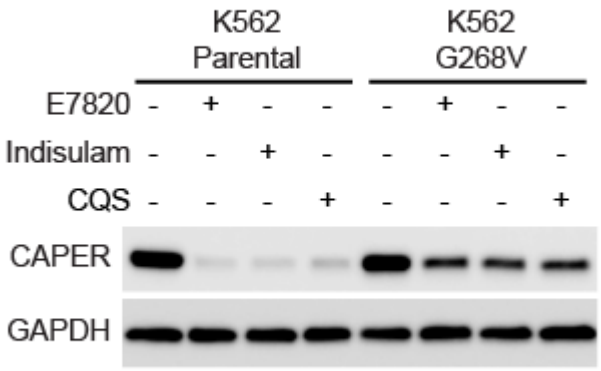

Figure II-17. Immunoblot analysis of parental and mutant K562 cells. Cells were treated with E7820 (3 μM), indisulam (3 μM), CQS (30 μM), or DMSO for 6 hours.

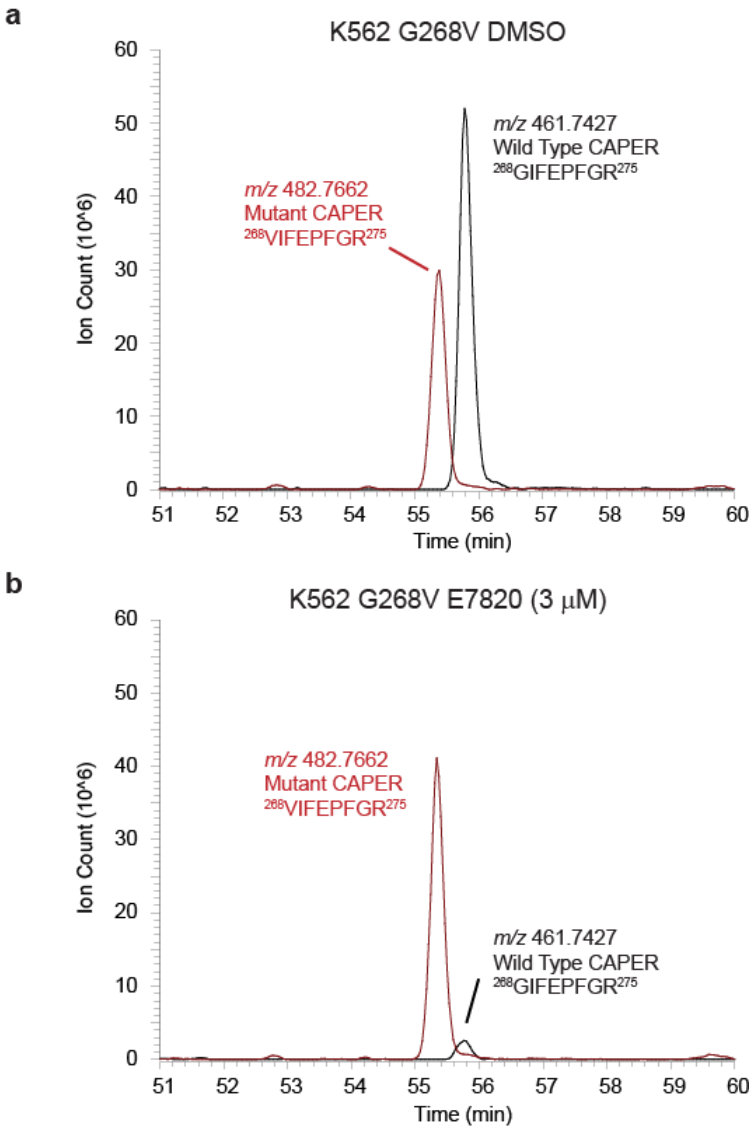

Figure II-18. Immunoprecipitation/LC-MS/MS analysis of CAPERα from K562-G278V cells. Cells were treated with (**a**) DMSO or (**b**) E7820 (3 μM) for 6 hours. Each chart shows a high-resolution mass chromatogram of the wild type and mutant CAPERα tryptic peptide from K562-G278V cells.

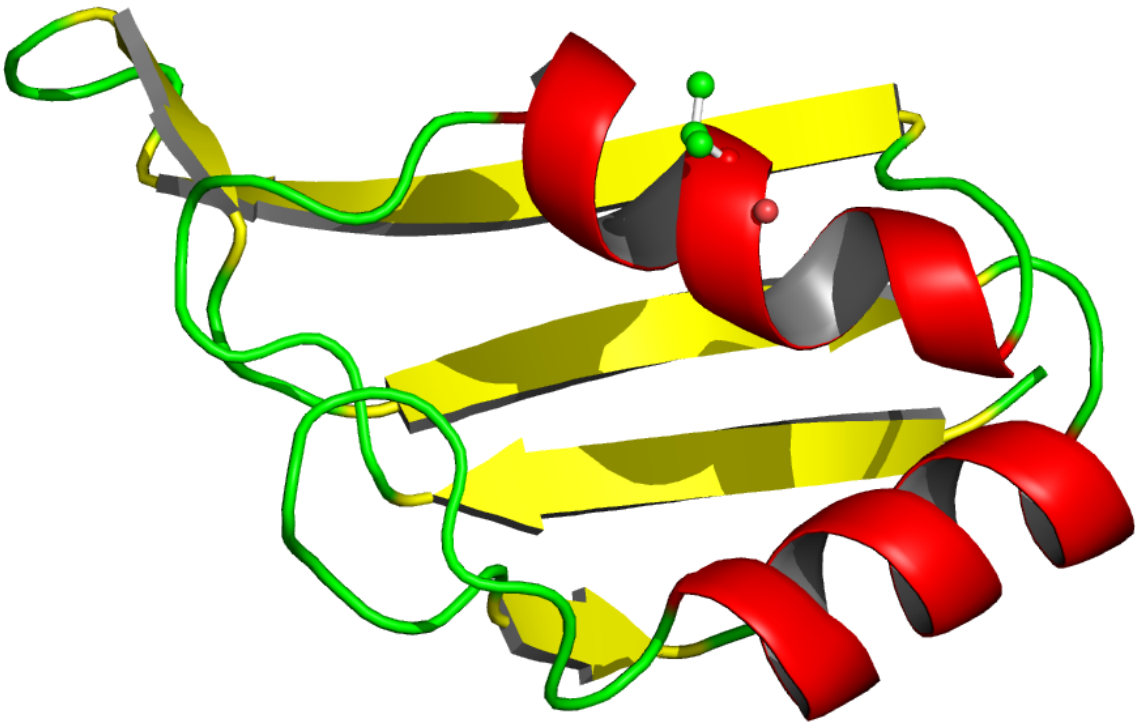

Figure II-19. NMR-based solution structure of CAPERα RNA recognition motif 2 (RRM2, PDB 2JRS), showing the substitution of ^{268}Glycine to Valine (ball and stick).

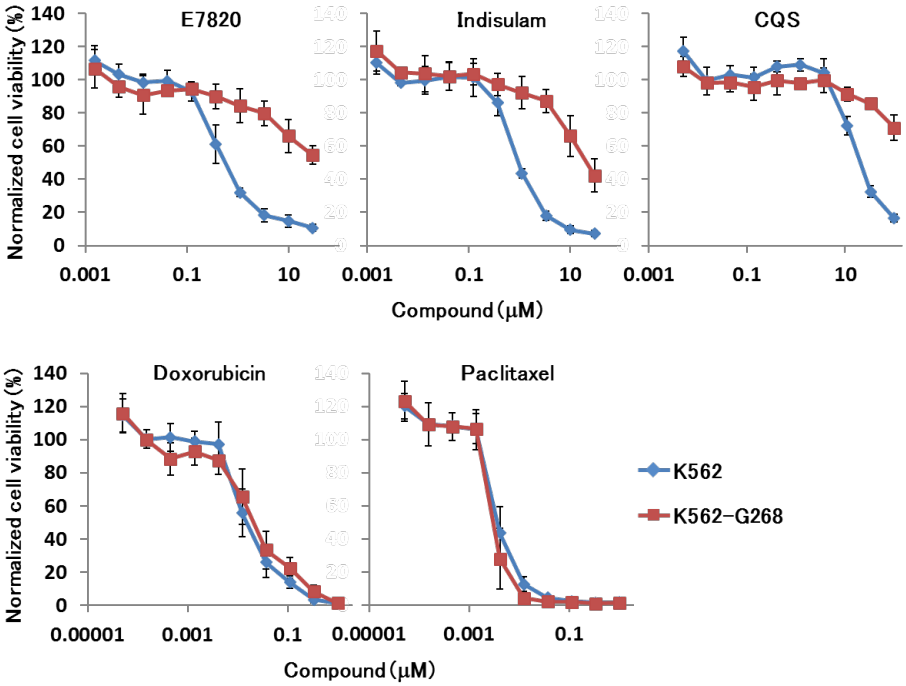

Figure II-20. Growth inhibitory activity of the anticancer sulfonamides and cytotoxic agents against parental K562 or K562-G268V cells. Data are presented as the mean of three independent experiments ± SD.

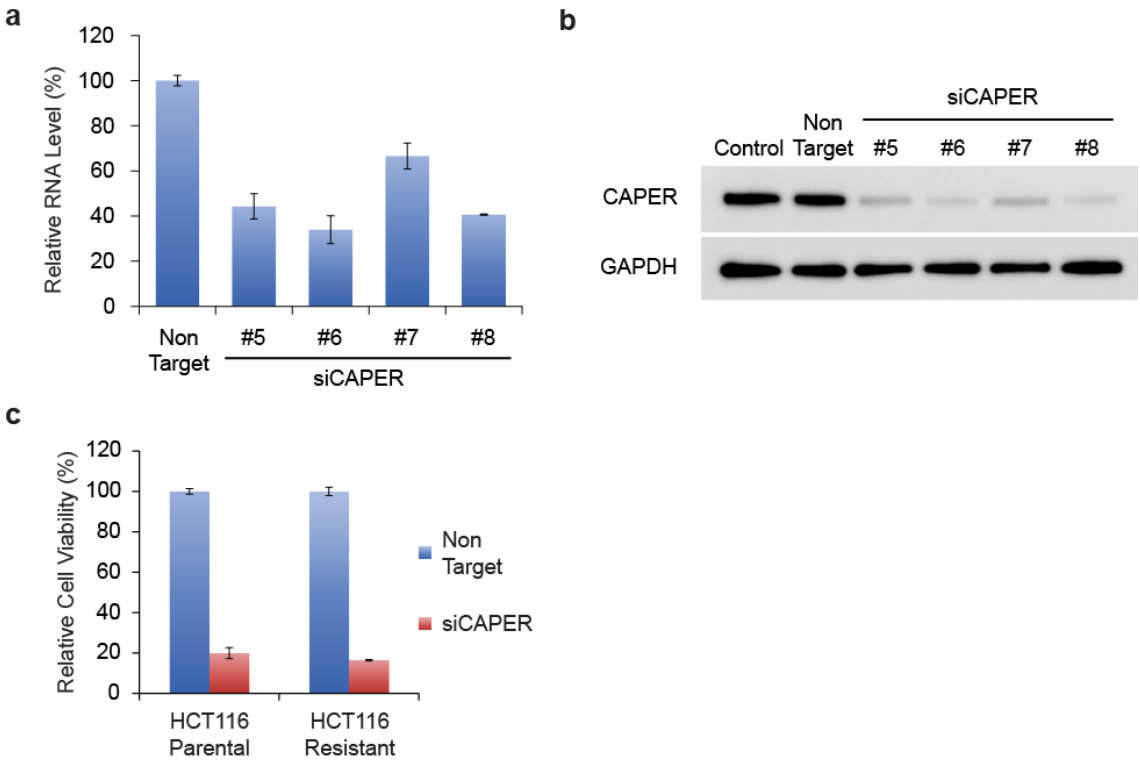

Figure II-21. Utilization of siRNA-mediated knockdown of CAPERα in HCT116 cells. (**a**) Effects of the knockdown of *CAPERα* mRNA assessed using quantitative polymerase chain reaction (qPCR) 48 hours after treatment with siRNA. Data are presented as mean ± SD (n = 3). (**b**) The reduction in CAPERα protein expression assessed by immunoblot 48 hours after treatment with siRNA. (**c**) The effect of siRNA-mediated *CAPERα* knockdown on parental or sulfonamide-resistant HCT116 cells. Data are presented as the mean ± SD (*n* = 3).

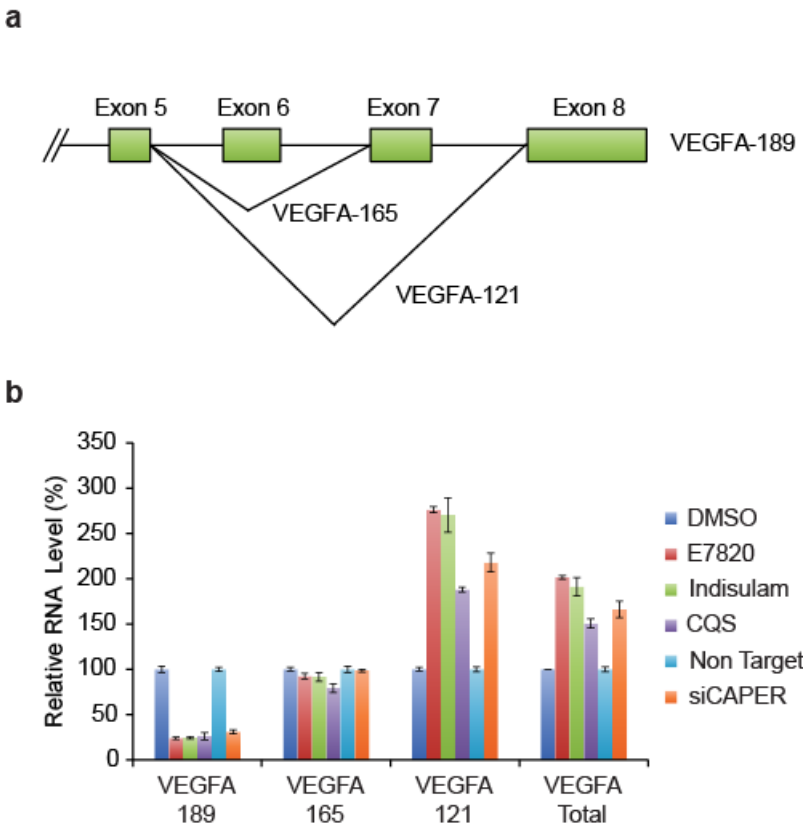

Figure II-22. Comparison of mRNA splicing modulation between the E7820-induced degradation and siRNA-mediated knockdown of *CAPERα*. (a) Correspondence between the exon-exon junctions and the splicing variants of VEGF-A. The PCR primers of exon junctions exon-5/6, exon-5/7, exon-5/8, and exon-2 correspond with the splicing variants VEGF-A-189, VEGF-A-165, VEGF-A-121, and total VEGF-A, respectively. (**b**) Exon junction targeted qPCR of VEGF-A in sulfonamide- or siRNA-treated HCT116 cells. Cells were treated with E7820 (3 μM), indisulam (3 μM), CQS (30 μM) or DMSO for 24 hours, or siRNA for 48 hours. Data are presented as the mean ± SD (n = 3).

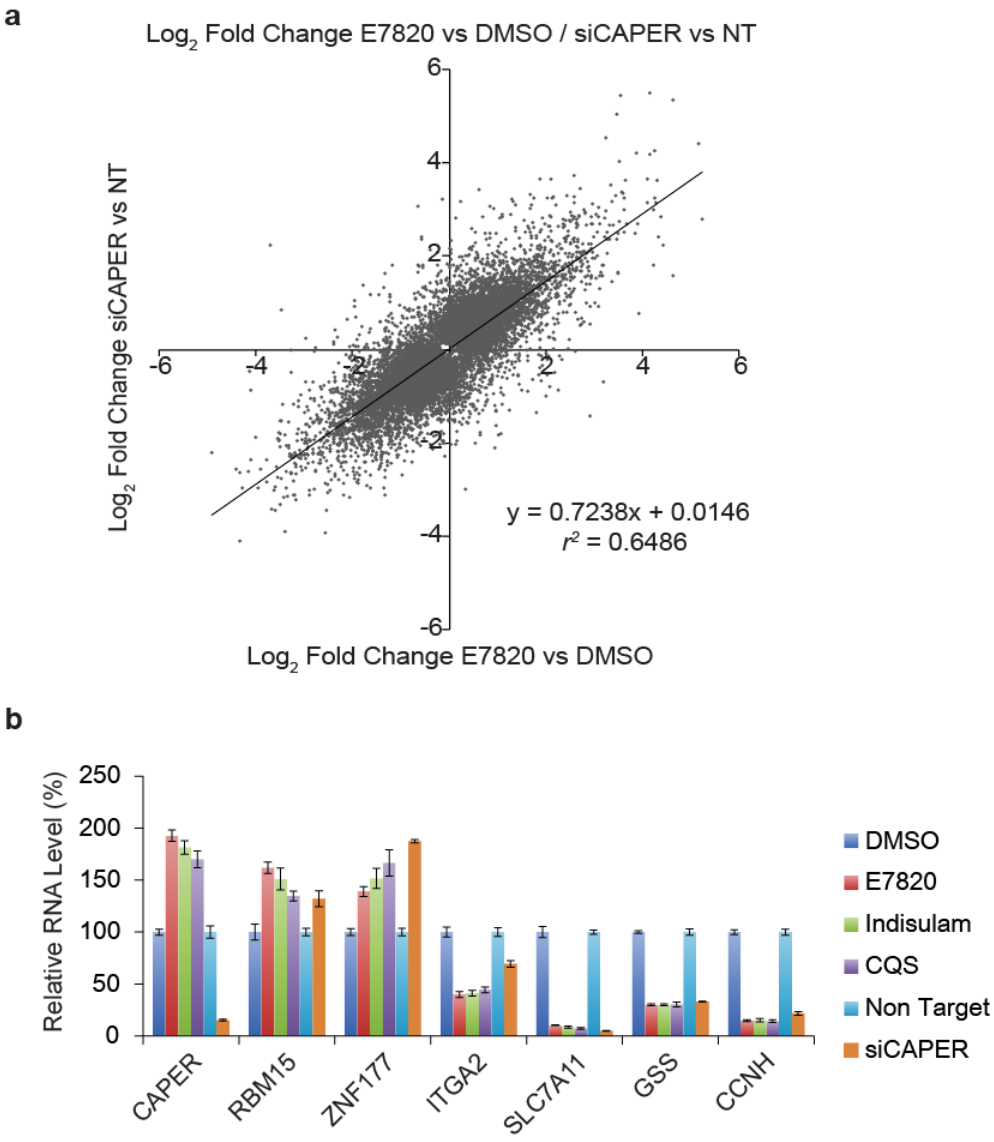

Figure II-23. Transcriptional comparison between the E7820-induced degradation and siRNA-mediated knockdown of *CAPERα*. (**a**) Cells were incubated with E7820 (1 μM) or DMSO for 24 hours, or siRNA for 48 hours to be analyzed by DNA microarray. Each point represents the $\log_2$ ratio of gene expression. Data are presented as the mean of biologically triplicate analyses, $P < 0.05$. (**b**) Gene expression of putative pharmacodynamic markers were assessed using quantitative polymerase chain reaction (qPCR). Cells were incubated with E7820 (3 μM), indisulam (3 μM), CQS (30μM), or

dimethyl sulfoxide (DMSO) for 24 hours, or siRNA for 48 hours. RNA levels of compounds and siCAPER treated cells were normalized with the RNA levels of DMSO control and non-target siRNA treated cells, respectively. The data are presented as mean ± SD (n = 3).

Tables

Table 1. Growth inhibitory activity of sulfonamide derivatives in HCT116 and K562 cells. The data are presented as the mean of three independent assays ± SD.

		Mean IC_{50} (μM)	SD (±)
HCT116	E7820	0.08	0.02
	Indisulam	0.18	0.02
	CQS	4.9	1.13
K562	E7820	0.54	0.15
	Indisulam	0.94	0.08
	CQS	20.55	2.49

Table 2. Summary of differential exome sequencing between parental HCT116 cells and spontaneously appearing sulfonamide-resistant clonal cells.

						Prental HCT116				Resistant Clone			
Gene	Chromosome	Position	Functions	Amino Acid Changes	Codon Change	Total Depth	Alteration Frequency (%)	Alteration Depth	Reference Depth	Total Depth	Alteration Frequency (%)	Alteration Depth	Reference Depth
CD8A	2	87015659	missense	**C217Y**	tGt/tAt	87	0	0	87	111	43.2	48	63
MON1A	3	49948000	stop-gained	**Q408***	Cag/Tag	115	0	0	115	107	60.7	65	42
SPOCK3	4	167713403	missense	**R212S**	agA/agT	99	0	0	99	138	47.8	66	72
PCDHGA1	5	140711186	missense	**Y312C**	tAc/tGc	132	0	0	132	157	49	77	80
MKRN1	7	140156549	missense	**R297C**	Cgc/Tgc	78	0	0	78	92	42.4	39	53
COL14A1	8	121357635	missense	**A1637V**	gCc/gTc	178	0	0	178	201	26.4	53	148
YY1	14	100706051	missense	**G157D**	gGc/gAc	136	0	0	136	155	50.3	78	77
SLFN11	17	33690713	missense	**Q38H**	caG/caC	134	0	0	134	173	42.8	74	99
NFE2L1	17	46136797	missense	**R705C**	Cgc/Tgc	240	0	0	240	275	30.2	83	192
BPTF	17	65928063	missense	**V2189M**	Gtg/Atg	259	0	0	259	337	31.8	107	230
ZNF461	19	37147428	missense	**P52A**	Cca/Gca	38	0	0	38	51	45.1	23	28
CEACAM6	19	42265405	missense	**R225C**	Cgc/Tgc	147	0	0	147	210	46.2	97	113
PLCB4	20	9318677	missense	**S63Y**	tCc/tAc	50	0	0	50	75	40	30	45
RBM39	20	34309684	missense	**G268V**	gGg/gTg	56	0	0	56	62	45.2	28	34
DLGAP4	20	35075259	stop-gained	**Q523***	Cag/Tag	54	0	0	54	76	53.9	41	35
SNX21	20	44462984	stop-gained	**R56***	Cga/Tga	155	0	0	155	197	42.1	83	114
CDH22	20	44803302	missense	**G777D**	gGc/gAc	110	0	0	110	116	56	65	51

Table 3. TaqMan Gene Expression Assays (Life Technologies) for Quantitative RT-PCR.

Gene name	Probe #
RBM39	Hs00705337_s1
ZNF177	Hs00185695_m1
RBM15	Hs00368498_s1
ITGA2	Hs00158148_m1
SLC7A11	Hs00204928_m1
GSS	Hs00609286_m1
CCNH	Hs00236923_m1
VEGFA (E5-E6)	Hs00903127_m1
VEGFA (E5-E7)	Hs00900057_m1
VEGFA (E5-E8)	Hs03929005_m1
VEGFA	Hs00900055_m1
DCAF15	Hs00384913_m1
DDB1	Hs01096550_m1
GAPDH	Hs99999905_m1

Supplementary Table 4. siRNA oligonucleotides.

Target gene	Catalog #	Target sequence
RBM39	J-011965-05	GAUAACAGCAGCAUAUGUA
RBM39	J-011965-06	GCAGGUGGUUUGCUGGUAA
RBM39	J-011965-07	GAUGGGAUACCGAGAUUAA
RBM39	J-011965-08	GACAGAAAUUCAAGACGUU
DCAF15	J-031237-15	UGGCGGACAGCGAGCGAUA
DCAF15	J-031237-16	UCACACUAGACUUCGAAUA
DCAF15	J-031237-17	CCUCCAAGGUCAUCGUCUU
DCAF15	J-031237-18	AUGAGUUGGAGGACGACAA
DDB1	J-012890-06	CACUAGAUCGCGAUAAUAA
DDB1	J-012890-07	GAAGGUUCUUUGCGGAUCA
DDB1	J-012890-08	CAUCGACGGUGACUUGAUU
DDB1	J-012890-09	CAUCUCGGCUCGUAUCUUG
CUL4A	J-012610-07	GCAUGUGGAUUCAAAGUUA
CUL4B	J-017965-08	GCUAUUGGCCGACAUAUGU
Non-targeting	D-001810-01-05	UGGUUUACAUGUCGACUAA

Table 5. Primers used in the amplicon sequencing.

RBM39-AmpliSeq-F	ACACTCTTTCCCTACACGACGCTCTTCCGATCTGGCTTTATGTGGGCTCATTAC
RBM39-AmpliSeq-R2	GTGACTGGAGTTCAGACGTGTGCTCTTCCGATCTATGTAGTTATACTCAGATCAACAACCTAC
DCAF15-1F-MiF	ACACTCTTTCCCTACACGACGCTCTTCCGATCTCCATTGCCAAAGCCAAGGAGTTTG
DCAF15-2R-MiR	GTGACTGGAGTTCAGACGTGTGCTCTTCCGATCTCGCTCACCATCCTCCGGCTCCGTC

Table 6. Primers used for indexing.

P5F	AATGATACGGCGACCACCGAGATCTACACTCTTTCCCTACACGACGCTCTTCCGATCT
P7R-Index1	CAAGCAGAAGACGGCATACGAGATCGTGATGTGACTGGAGTTCAGACGTGTGCTCTTCCGATCT
P7R-Index14	CAAGCAGAAGACGGCATACGAGATGGAACTGTGACTGGAGTTCAGACGTGTGCTCTTCCGATCT
P7R-Index15	CAAGCAGAAGACGGCATACGAGATTGACATGTGACTGGAGTTCAGACGTGTGCTCTTCCGATCT
P7R-Index16	CAAGCAGAAGACGGCATACGAGATGGACGGGTGACTGGAGTTCAGACGTGTGCTCTTCGATCT
P7R-Index18	CAAGCAGAAGACGGCATACGAGATGCGGACGTGACTGGAGTTCAGACGTGTGCTCTTCCGATCT

Chapter III

Concluding remarks

Regulation of protein degradation is an essential mechanism to maintain cell homeostasis and to regulate cell fate. Ubiquitin is well conserved and widely distributed 76 amino-acid tag of protein, and the protein ubiquitination is responsible for much of the regulated proteolysis in the cell. In spite of large efforts to control ubiquitin ligase by a small molecule as attempts for drug discovery and development, only a few drugs which targets the ubiquitin system have been approved[50,51].

In chapter II, I revealed the anticancer mechanism of a series of the sulfonamide small compounds which are developed as a candidate of pharmaceutical drug because they show anticancer activities in preclinical models and clinical benefits in a small subset of patients but the primary target molecule and mechanism of action is not understood. I revealed those sulfonamide derivatives inducing protein complex assembly between CAPERα and $CRL4^{DCAF15}$ to lead the ubiquitination and proteasomal degradation of a splicing factor CAPERα[s]. A single amino acid substitution of CAPERα conferred resistance against sulfonamide-induced CAPERα degradation and cell-growth inhibition, suggesting that CAPERα degradation is a key biochemical activity that

underlies the anticancer properties of these compounds. CAPERα is known to have similar protein motifs with U2AF2 splicing factor and to regulate divers RNA splicing events[32,35]. I confirmed chemical knockdown of *CAPERα* by E7820 induces the significant change in the alternative splicing of VEGFA and the broad gene expression changes which may cause anti-proliferative effect in cells. Thus, the anticancer mechanism of the sulfonamide derivatives, in addition to the mechanism of IMiDs, demonstrates a novel feature of the ubiquitin ligase as a target of small molecule ligands that induce selective protein ubiquitination and degradation to regulate gene expression, mRNA splicing, and cell fate.

Acknowledgments

Most of the content of this dissertation was previously published in Nature Chemical Biology (No. 13, Vol. 6, 675-680)[8].

I wish to thank for all who provided me the kind support, guidance, and encouragement throughout my research work. Most of all, I want to express my deep gratitude to Professor Akiyoshi Fukamizu for his supports and advises in preparing this dissertation. I am very grateful to Dr. Benjamin F. Cravatt and Dr. Bruce A. Littlefield for helpful advises and comments in preparing research article. I am indebted to Dr. Takashi Owa and all other members of anti-cancer sulfonamide projects in Eisai Co.,Ltd., past and now, for their efforts in drug discovery and development. Finally, I owe this thesis to my wife and sons.

References

1 Dang, C. V., Reddy, E. P., Shokat, K. M. & Soucek, L. Drugging the 'undruggable' cancer targets. *Nature reviews. Cancer* **17**, 502-508, doi:10.1038/nrc.2017.36 (2017).

2 Wu, S. Y., Lopez-Berestein, G., Calin, G. A. & Sood, A. K. RNAi therapies: drugging the undruggable. *Sci Transl Med* **6**, 240ps247, doi:10.1126/scitranslmed.3008362 (2014).

3 Chen, D., Frezza, M., Schmitt, S., Kanwar, J. & Dou, Q. P. Bortezomib as the first proteasome inhibitor anticancer drug: current status and future perspectives. *Curr Cancer Drug Targets* **11**, 239-253 (2011).

4 Ito, T. *et al.* Identification of a primary target of thalidomide teratogenicity. *Science* **327**, 1345-1350, doi:10.1126/science.1177319 (2010).

5 Kronke, J. *et al.* Lenalidomide causes selective degradation of IKZF1 and IKZF3 in multiple myeloma cells. *Science* **343**, 301-305, doi:10.1126/science.1244851 (2014).

6 Lu, G. *et al.* The myeloma drug lenalidomide promotes the cereblon-dependent destruction of Ikaros proteins. *Science* **343**, 305-309, doi:10.1126/science.1244917 (2014).

7 Kronke, J. *et al.* Lenalidomide induces ubiquitination and degradation of

CK1alpha in del(5q) MDS. *Nature* **523**, 183-188, doi:10.1038/nature14610 (2015).

8 Uehara, T. *et al.* Selective degradation of splicing factor CAPERalpha by anticancer sulfonamides. *Nat Chem Biol* **13**, 675-680, doi:10.1038/nchembio.2363 (2017).

9 Soucy, T. A. *et al.* An inhibitor of NEDD8-activating enzyme as a new approach to treat cancer. *Nature* **458**, 732-736, doi:10.1038/nature07884 (2009).

10 Kim, K. B. & Crews, C. M. From epoxomicin to carfilzomib: chemistry, biology, and medical outcomes. *Nat Prod Rep* **30**, 600-604, doi:10.1039/c3np20126k (2013).

11 Fischer, E. S. *et al.* Structure of the DDB1-CRBN E3 ubiquitin ligase in complex with thalidomide. *Nature* **512**, 49-53, doi:10.1038/nature13527 (2014).

12 Chamberlain, P. P. *et al.* Structure of the human Cereblon-DDB1-lenalidomide complex reveals basis for responsiveness to thalidomide analogs. *Nat Struct Mol Biol* **21**, 803-809, doi:10.1038/nsmb.2874 (2014).

13 Petzold, G., Fischer, E. S. & Thoma, N. H. Structural basis of lenalidomide-induced CK1alpha degradation by the CRL4(CRBN) ubiquitin ligase. *Nature* **532**, 127-130, doi:10.1038/nature16979 (2016).

14 Matyskiela, M. E. *et al.* A novel cereblon modulator recruits GSPT1 to the CRL4(CRBN) ubiquitin ligase. *Nature* **535**, 252-257, doi:10.1038/nature18611 (2016).

15 Jin, J., Arias, E. E., Chen, J., Harper, J. W. & Walter, J. C. A family of diverse Cul4-Ddb1-interacting proteins includes Cdt2, which is required for S phase destruction of the replication factor Cdt1. *Mol Cell* **23**, 709-721, doi:10.1016/j.molcel.2006.08.010 (2006).

16 Lee, J. & Zhou, P. DCAFs, the missing link of the CUL4-DDB1 ubiquitin ligase. *Mol Cell* **26**, 775-780, doi:10.1016/j.molcel.2007.06.001 (2007).

17 Hannah, J. & Zhou, P. Distinct and overlapping functions of the cullin E3 ligase scaffolding proteins CUL4A and CUL4B. *Gene* **573**, 33-45, doi:10.1016/j.gene.2015.08.064 (2015).

18 Winter, G. E. *et al.* DRUG DEVELOPMENT. Phthalimide conjugation as a strategy for in vivo target protein degradation. *Science* **348**, 1376-1381, doi:10.1126/science.aab1433 (2015).

19 Lu, J. *et al.* Hijacking the E3 Ubiquitin Ligase Cereblon to Efficiently Target BRD4. *Chem Biol* **22**, 755-763, doi:10.1016/j.chembiol.2015.05.009 (2015).

20 Zengerle, M., Chan, K. H. & Ciulli, A. Selective Small Molecule Induced

Degradation of the BET Bromodomain Protein BRD4. *ACS Chem Biol* **10**, 1770-1777, doi:10.1021/acschembio.5b00216 (2015).

21 Bondeson, D. P. *et al.* Catalytic in vivo protein knockdown by small-molecule PROTACs. *Nat Chem Biol* **11**, 611-617, doi:10.1038/nchembio.1858 (2015).

22 Toure, M. & Crews, C. M. Small-Molecule PROTACS: New Approaches to Protein Degradation. *Angew Chem Int Ed Engl* **55**, 1966-1973, doi:10.1002/anie.201507978 (2016).

23 Miller, V. A. *et al.* Phase II trial of chloroquinoxaline sulfonamide (CQS) in patients with stage III and IV non-small-cell lung cancer. *Cancer Chemother Pharmacol* **40**, 415-418, doi:10.1007/s002800050679 (1997).

24 Baur, M., Gneist, M., Owa, T. & Dittrich, C. Clinical complete long-term remission of a patient with metastatic malignant melanoma under therapy with indisulam (E7070). *Melanoma Res* **17**, 329-331, doi:10.1097/CMR.0b013e3282ef4189 (2007).

25 Mita, M. *et al.* Phase I study of E7820, an oral inhibitor of integrin alpha-2 expression with antiangiogenic properties, in patients with advanced malignancies. *Clin Cancer Res* **17**, 193-200, doi:10.1158/1078-0432.CCR-10-0010 (2011).

26 Ozawa, Y. *et al.* E7070, a novel sulphonamide agent with potent antitumour activity in vitro and in vivo. *Eur J Cancer* **37**, 2275-2282 (2001).

27 Funahashi, Y. *et al.* Sulfonamide derivative, E7820, is a unique angiogenesis inhibitor suppressing an expression of integrin alpha2 subunit on endothelium. *Cancer Res* **62**, 6116-6123 (2002).

28 Yokoi, A. *et al.* Profiling novel sulfonamide antitumor agents with cell-based phenotypic screens and array-based gene expression analysis. *Mol Cancer Ther* **1**, 275-286 (2002).

29 Abbate, F., Casini, A., Owa, T., Scozzafava, A. & Supuran, C. T. Carbonic anhydrase inhibitors: E7070, a sulfonamide anticancer agent, potently inhibits cytosolic isozymes I and II, and transmembrane, tumor-associated isozyme IX. *Bioorg Med Chem Lett* **14**, 217-223 (2004).

30 Semba, T. *et al.* An angiogenesis inhibitor E7820 shows broad-spectrum tumor growth inhibition in a xenograft model: possible value of integrin alpha2 on platelets as a biological marker. *Clin Cancer Res* **10**, 1430-1438 (2004).

31 Venable, J. D., Dong, M. Q., Wohlschlegel, J., Dillin, A. & Yates, J. R. Automated approach for quantitative analysis of complex peptide mixtures from tandem mass spectra. *Nat Methods* **1**, 39-45, doi:10.1038/nmeth705 (2004).

32 Imai, H., Chan, E. K., Kiyosawa, K., Fu, X. D. & Tan, E. M. Novel nuclear autoantigen with splicing factor motifs identified with antibody from hepatocellular carcinoma. *J Clin Invest* **92**, 2419-2426, doi:10.1172/JCI116848 (1993).

33 Higa, L. A., Mihaylov, I. S., Banks, D. P., Zheng, J. & Zhang, H. Radiation-mediated proteolysis of CDT1 by CUL4-ROC1 and CSN complexes constitutes a new checkpoint. *Nat Cell Biol* **5**, 1008-1015, doi:10.1038/ncb1061 (2003).

34 Jung, D. J., Na, S. Y., Na, D. S. & Lee, J. W. Molecular cloning and characterization of CAPER, a novel coactivator of activating protein-1 and estrogen receptors. *J Biol Chem* **277**, 1229-1234, doi:10.1074/jbc.M110417200 (2002).

35 Dowhan, D. H. *et al.* Steroid hormone receptor coactivation and alternative RNA splicing by U2AF65-related proteins CAPERalpha and CAPERbeta. *Mol Cell* **17**, 429-439, doi:10.1016/j.molcel.2004.12.025 (2005).

36 Loerch, S., Maucuer, A., Manceau, V., Green, M. R. & Kielkopf, C. L. Cancer-relevant splicing factor CAPERalpha engages the essential splicing factor SF3b155 in a specific ternary complex. *J Biol Chem* **289**, 17325-17337,

doi:10.1074/jbc.M114.558825 (2014).

37 Kang, Y. K. *et al.* CAPER is vital for energy and redox homeostasis by integrating glucose-induced mitochondrial functions via ERR-alpha-Gabpa and stress-induced adaptive responses via NF-kappaB-cMYC. *PLoS Genet* **11**, e1005116, doi:10.1371/journal.pgen.1005116 (2015).

38 Huang, G., Zhou, Z., Wang, H. & Kleinerman, E. S. CAPER-alpha alternative splicing regulates the expression of vascular endothelial growth factor(1)(6)(5) in Ewing sarcoma cells. *Cancer* **118**, 2106-2116, doi:10.1002/cncr.26488 (2012).

39 Sveen, A., Kilpinen, S., Ruusulehto, A., Lothe, R. A. & Skotheim, R. I. Aberrant RNA splicing in cancer; expression changes and driver mutations of splicing factor genes. *Oncogene* **35**, 2413-2427, doi:10.1038/onc.2015.318 (2016).

40 Tan, X. *et al.* Mechanism of auxin perception by the TIR1 ubiquitin ligase. *Nature* **446**, 640-645, doi:10.1038/nature05731 (2007).

41 Wisniewski, J. R., Zougman, A., Nagaraj, N. & Mann, M. Universal sample preparation method for proteome analysis. *Nat Methods* **6**, 359-362, doi:10.1038/nmeth.1322 (2009).

42 Egertson, J. D., MacLean, B., Johnson, R., Xuan, Y. & MacCoss, M. J.

Multiplexed peptide analysis using data-independent acquisition and Skyline. *Nat Protoc* **10**, 887-903, doi:10.1038/nprot.2015.055 (2015).

43 Mali, P. *et al.* RNA-guided human genome engineering via Cas9. *Science* **339**, 823-826, doi:10.1126/science.1232033 (2013).

44 Cong, L. *et al.* Multiplex genome engineering using CRISPR/Cas systems. *Science* **339**, 819-823, doi:10.1126/science.1231143 (2013).

45 Li, H. & Durbin, R. Fast and accurate short read alignment with Burrows-Wheeler transform. *Bioinformatics* **25**, 1754-1760, doi:10.1093/bioinformatics/btp324 (2009).

46 McKenna, A. *et al.* The Genome Analysis Toolkit: a MapReduce framework for analyzing next-generation DNA sequencing data. *Genome Res* **20**, 1297-1303, doi:10.1101/gr.107524.110 (2010).

47 Hazeldine, S. T. *et al.* Design, synthesis, and biological evaluation of analogues of the antitumor agent, 2-(4-[(7-chloro-2-quinoxalinyl)oxy]phenoxy)propionic acid (XK469). *J Med Chem* **44**, 1758-1776 (2001).

48 Owa, T. Chemistry and Biology of a Series of Antitumor Sulfonamides: Exploiting Transcriptomic and Quantitative Proteomic Analyses for Exploring Druggable Chemical SpaceChemistry and Biology of a Series of Antitumor

Sulfonamides: Exploiting Transcriptomic and Quantitative Proteomic Analyses for Exploring Druggable Chemical Space. *Yuki Gosei Kagaku Kyokaishi* **64**, 1171-1179 (2006).

49 Oda, Y. *et al.* Quantitative chemical proteomics for identifying candidate drug targets. *Anal Chem* **75**, 2159-2165, doi:10.1021/ac026196y (2003).

50 Nalepa, G., Rolfe, M. & Harper, J. W. Drug discovery in the ubiquitin-proteasome system. *Nature reviews. Drug discovery* **5**, 596-613, doi:10.1038/nrd2056 (2006).

51 Huang, X. & Dixit, V. M. Drugging the undruggables: exploring the ubiquitin system for drug development. *Cell research* **26**, 484-498, doi:10.1038/cr.2016.31 (2016).